Manuscript Details

Manuscript number YBENG_2017_787

Title Performance of Continuous Flat Plate Biofilm Photobioreactors of Circular and Rectangular Configurations: Mathematical Modeling

Abstract

Flat plate photobioreactors (FPPBRs) using bacterial biofilm have gained much attention due to operational ease, improved light conversion efficiency and reduction of process cost, particularly in hydrogen production. In this study, two comprehensive mathematical models, one explaining the dynamics of a batch type FPPBR used for the development of biofilm and the other deterministic model (both temporal and spatial) to predict the performance of a continuous FPPBR using Rhodopseudomonas sp have been developed for both circular and rectangular configurations. The system equations have been solved using MATLAB 2014. From batch studies, the maximum specific growth rate and half saturation constant for the microorganism have been determined to be 0.07h-1 and 1.946g/L respectively. An “Instantaneous attachment and proliferation” mechanism has been proposed to explain the behavior of biofilm right from the early stage of attachment to the reversal from attached to planktonic state. The flow patterns of substrate medium through the biofilm have been generated using COMSOL Multiphysics. From the perspective of the hydrogen yield, the models predict that the FPPBR geometry plays a crucial role by demonstrating the superior performance of the circular reactor in comparison to the rectangular counterpart. It is expected that the mathematical models developed under the present study will help in the design, scale-up and control of FPPBRs to be used particularly for hydrogen production using suitable microorganisms.

Submission Files Included in this PDF

File Name [File Type]

Highlights.docx [Highlights]

Graphical abstract.tif [Graphical Abstract]

Manuscript.docx [Manuscript File]

Figure 1.tif [Figure]

Figure 2.tif [Figure]

Figure 3.tif [Figure]

Figure 4.tif [Figure]

Figure 5.tif [Figure]

Figure 6.tif [Figure]

Figure 7.tif [Figure]

Figure 8.tif [Figure]

Figure 9.tif [Figure]

Figure 10.tif [Figure]

Figure 11.tif [Figure]

Figure 12.tif [Figure]

To view all the submission files, including those not included in the PDF, click on the manuscript title on your EVISE Homepage, then click 'Download zip file'.

Highlights

- Two biofilm type FPPBR systems have been mathematically modelled.
- A biosystem of H_2 producing immobilized *Rhodopseudomonas sp*. has been studied.
- Dynamics of *Rhodopseudomonas sp.* biofilm formation has been demonstrated.
- Effect of design geometry on the H_2 production performance of the FPPBR has been investigated.
- H_2 production in circular configuration of the FPPBR has been found to be much better than the rectangular counterpart.

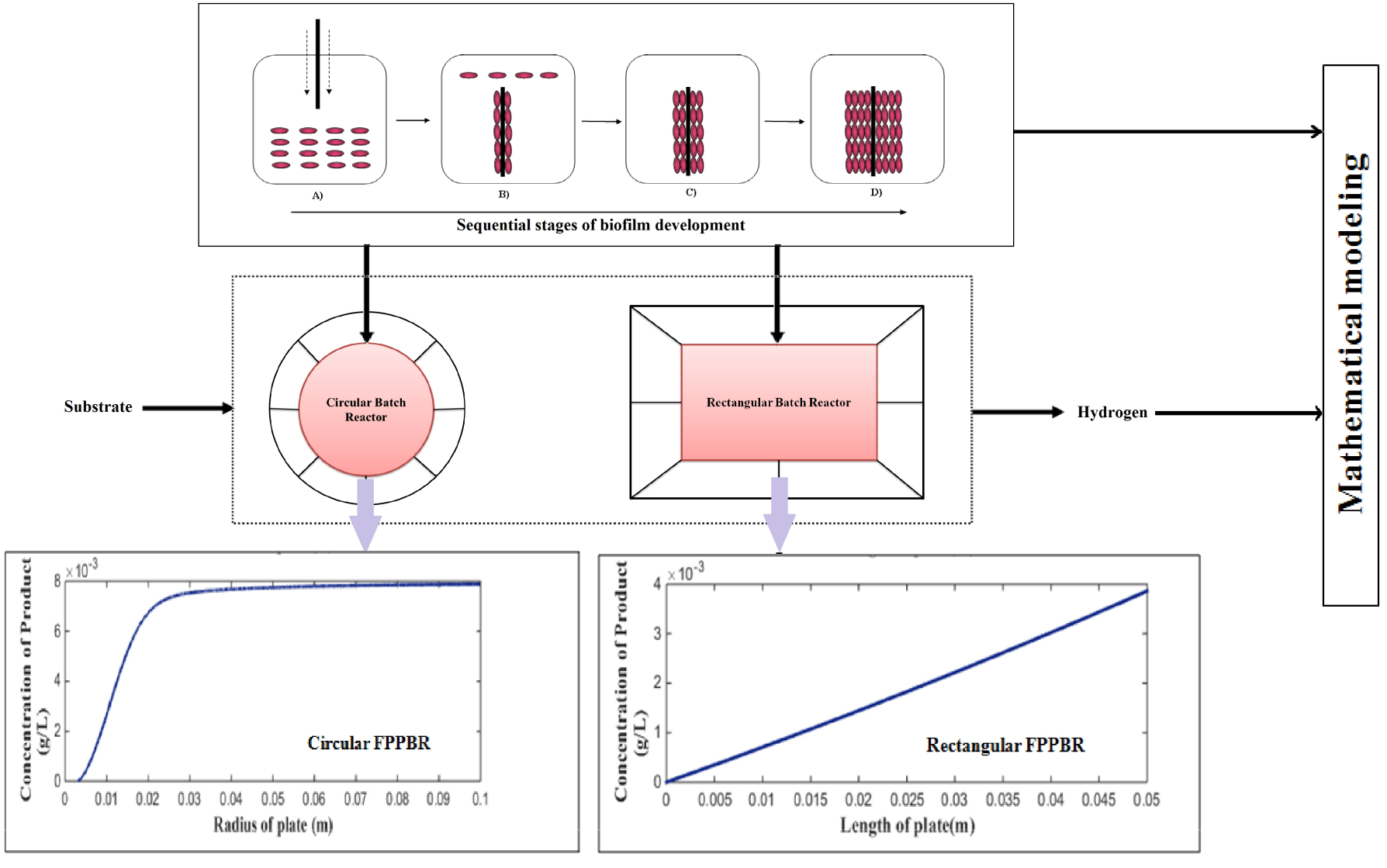
A)
B)
C)
D)
Sequential stages of biofilm development
Substrate
Circular Batch Reactor
Rectangular Batch Reactor
Hydrogen
Mathematical modeling
Concentration of Product (g/L)
×10^-3
Circular FPPBR
Radius of plate (m)
Concentration of Product (g/L)
×10^-3
Rectangular FPPBR
Length of plate(m)

Performance of Continuous Flat Plate Biofilm Photobioreactors of Circular and Rectangular Configurations: Mathematical Modeling

Arit Das[a], Sankhadeep Basu[a], Shiladitya Ghosh[a], Ranjana Chowdhury[a,*]

[a]Chemical Engineering Department, Jadavpur University, Kolkata 700032, India

*Corresponding Author

Tel: +91 332414 6378

E-mail: ranjana.juchem@gmail.com (Dr. Ranjana Chowdhury)

ABSTRACT

Flat plate photobioreactors (FPPBRs) using bacterial biofilm have gained much attention due to operational ease, improved light conversion efficiency and reduction of process cost, particularly in hydrogen production. In this study, two comprehensive mathematical models, one explaining the dynamics of a batch type FPPBR used for the development of biofilm and the other deterministic model (both temporal and spatial) to predict the performance of a continuous FPPBR using *Rhodopseudomonas sp* have been developed for both circular and rectangular configurations. The system equations have been solved using MATLAB 2014. From batch studies, the maximum specific growth rate and half saturation constant for the microorganism have been determined to be $0.07h^{-1}$ and 1.946g/L respectively. An "Instantaneous attachment and proliferation" mechanism has been proposed to explain the behavior of biofilm right from the early stage of attachment to the reversal from attached to planktonic state. The flow patterns of substrate medium through the biofilm have been generated using COMSOL Multiphysics. From the perspective of the hydrogen yield, the models predict that the FPPBR geometry plays a crucial role by demonstrating the superior performance of the circular reactor in comparison to the rectangular counterpart. It is expected that the mathematical models developed under the present study will help in the design, scale-up and control of FPPBRs to be used particularly for hydrogen production using suitable microorganisms.

Keywords: Flat plate photobioreactor; Circular and rectangular configuration; Mathematical modeling; Biofilm development; Continuous operation; Hydrogen production using PNSB

41 ## 1. Introduction

42 ### *1.1. Flat Plate Photobioreactors (FPPBRs) and existing Mathematical Models*

43 PBRs have been exclusively used for bioprocesses using phototrophic organisms, namely, algae,
44 cyanobacteria, purple non-sulfur bacteria (PNSB), etc. Apart from the usual design criteria like
45 uniform stirring, availability of high surface area for interphase transfer of substrates and
46 metabolites of conventional bioreactors, one of the key factors of PBR design is ensuring the
47 proper distribution and conversion efficiency of light. Stirred-tank (Skjanes, Knutsen, Kallqvist,
48 Lindblad, 2008; Berberoglu, Yin, Pilon, 2007), tubular (Molina, Fernandez, Acien, Chisti, 2001;
49 Dasgupta et al., 2010), vertical-column (Xu et al. 2002; Janssen, Tramper, Mur, Wijffels, 2003)
50 and flat plate PBRs and flat plate photobio-bubble reactor (Pradhan, Bhattacharjee, Mitra,
51 Bhattacharya, Chowdhury, 2015) are some of the existing PBR designs which have received
52 much attention in the recent past. However, tubular and vertical column PBRs suffers from
53 problems regarding scale up (Molina et al., 2001) and small illumination area (Miron, Gomez,
54 Camacho, Molina, Chisti, 1999) respectively. In this context, FPPBRs have been observed to be
55 a cheaper alternative to the aforementioned configurations (Lehr & Posten, 2009) offering better
56 control and decent photosynthetic efficiency (Richmond, 2010; Hu, Gutermann, Richmond,
57 1996) due to their high surface to volume ratio (Akkerman, Janssen, Rocha, Wijffels, 2002) and
58 shorter light penetration length. Along with the use of suspended culture, researchers have also
59 used attached biofilms in FPPBRs. Through the employment of biofilm, cost incurred in the
60 downstream processing, i.e., the separation of biomass from the products and unconverted
61 substrate existing in the extracellular medium, is reduced (Gross & Wen, 2014; Irving & Allen,
62 2011). Attached biofilms FPPBRs have been widely employed for harvesting microalgae. The
63 flat plate biofilm PBR, suspended solid phase PBR (Zhuang, Hu, Wu, Wang, Zhang, 2014),

revolving algal biofilm reactor (Gross & Wen 2014), waveguide reactor (Genin, Aitchison, Allen, 2015), rocking (Johnson & Wen, 2010), vertical plate (Liu et al., 2013), flat plate reactor using gas lift (Tamburic, Zemichael, Crudge, Maitland, Hellgardt, 2011), rotating algal biofilm reactor (Christenson & Sims, 2012), airlift PBR (Tao et al., 2017) and an attached growth membrane reactor (Li, Suwanate, Visvanathan, 2017) have yielded promising results. A simplistic design of an algal biofilm PBR was developed where a concrete slab was used as the biofilm growth surface (Ozkan, Kinney, Katz, Berberoglu, 2012). Cultivation of microalgae has also been rigorously modeled FPPBRs. An FPPBR using biofilm of marine microalgae was kinetically modeled and the effect of model parameters on the predicted performance was studied (He et al., 2016). An adaptable model scheme for controlling the irradiance in an FPPBR has been reported to enhance the microalgal growth and biomass productivity (Kandilian, Tsao, Pilon, 2014). The cultivation of microalgae in an FPPBR provided with internal baffles was investigated and the flow and particle trajectories were analyzed using CFD approach (Zhang et al., 2013). A membrane FPPBR using algal biofilm was mathematically modeled (Li et al., 2017). The phototrophic growth of algae in a lab-scale FPPBR was studied and different growth models describing the kinetics associated with the process was developed (Koller, Löwe, Schmid, Mundt, Weuster-Botz, 2017).

FPPBRs using biofilms of photoheterotrophic bacteria are also in current practice (Ghosh, Dairkee, Chowdhury, Bhattacharya, 2016; Wu, Hay, Kong, Juan, Jahim 2012; Adessi, Torzillo, Baccetti, De Philippis 2012). Although in many bacterial FPPBRs, biofilms are developed on suspended solid matrices, a new trend is coming up where the biofilm is developed on transparent glass plates of rectangular or circular shape (Zagrodnik, Thiel, Seifert, Włodarczak, Łaniecki, 2013; Zagrodnik, Seifert, Stodolny, Laniecki, 2015). This type of reactor design

facilitates the uniform distribution of light and can reduce the chance of detachment of biofilm from the solid matrix. It is understandable that mathematical modeling of FPPBRs employing biofilm of PNSB systems is required to clarify the influence of in-situ biochemical processes occurring in the biofilm on the ex-situ impacts of operating parameters on product yields. Mathematical models can only elucidate the complex characteristics of bacterial biofilms which is almost beyond the scope of experimental understanding (Tang & Liu, 2017).

The mathematical models of FPPBR are important from the perspective of scaling-up and control of lab-scale bioreactors. A realistic mathematical model for an FPPBR can only be developed through the consolidated employment of classical chemical, biochemical and bioprocess engineering knowledge. The growth of biofilm formation complexities of a PNSB, namely, *Rhodobacter sphaeroides* using a two-dimensional model of a growing biofilm has been mathematically represented by adjusting the Mimura-Sakaguchi-Matsushita's bacterial colony model (Ward et al., 2005). An interesting mathematical model of a flat panel biofilm photobioreactor using *Rhodopseudomonas* sp. has been developed for a rectangular bioreactor of simulation dimension of 2mmX0.4mm using cellular automaton rule and diffusion reaction equations (Liao et al., 2012). In this case during modeling it was assumed that the solid surface was covered with biofilm during inoculation; to which substrate was transferred through convection and diffusion for further growth of biofilm through microbial reactions. Sometimes, prior to the continuous operation of an FPPBR, biofilm can be developed in another FPPBR run in batch mode by immersing a glass disk in a growth medium containing suspended microbial cells (Zagrodnik et al., 2013; Zagrodnik et al., 2015). No mathematical model of batch type FPPBR, used for the biofilm development, is currently available to the best of our knowledge. A simplistic mathematical representation for the underlying mechanism of attachment of the

suspended cells on to the glass surface is necessary for the modeling of the batch type FPPBR where the biofilm is developed. Although the use of continuous FPPBR of circular configuration using PNSB has also been reported, no information on the mathematical model of such reactor is available (Zagrodnik et al., 2013). Although many mathematical models have been developed for algal FPPBR, only one pioneering research study has been reported on the modeling of continuous rectangular FPPBR using bacterial biofilm (Liao et al., 2012). The model is restricted to the rectangular configuration of reactor and is not applicable for systems where the biofilm is developed in batch reactors by immersing the solid matrix in bacterial culture. Therefore, mathematical models should also be developed for the batch reactors where there is a switching of microbial growth from suspended to planktonic forms and for continuous FPPBR where the hydrodynamics concerned with the circular configuration has to be accounted.

In this work, we have modeled the system dynamics of rectangular and circular batch FPPBRs using glass plates for the development of biofilm. The surface area available for the growth of biofilm has been maintained equal in the circular and the rectangular counterparts for comparing their performance. The deterministic mathematical models for continuous flow FPPBRs using the biofilm developed in the corresponding batch reactors have also been developed. As a case study of the FPPBR system, the production of hydrogen using biofilm of *Rhodopseudomonas sp* on rectangular and circular glass plates has been considered. The simulated results have been compared with the literature data, wherever possible.

1.2. Base case photofermentation system of Rhodopseudomonas sp biofilm

According to the protocol followed in a previous investigation (Zagrodnik et al., 2013), the biofilm of *Rhodopseudomonas sp* was developed on both faces of the glass plate in a batch

reactor using malic acid as the substrate. Subsequently, the glass plate holding the attached biofilm of *Rhodopseudomonas sp* was used in a continuous PBR for hydrogen production. Under the present investigation both the batch and continuous reactors have been mathematically modeled. A deterministic mathematical model for a circular flat plate continuous PBR, as utilized in the aforementioned work (Zagrodnik et al., 2013) has been developed.

The model scheme showing the input and output variables along with model constants is represented in Figure 1.

1.3. Formation of Biofilm of Rhodopseudomonas sp by "Instantaneous Attachment and Proliferation" Mechanism

A few experimental studies on photofermentative H_2 production from biofilm type immobilized systems have been performed using the PNSB *Rhodobacter sphaeroides* (Zagrodnik et al., 2015; Xie et al., 2012; Zhang et al., 2010; Tian et al., 2009). However, detailed demonstration of the developmental stages of PNSB biofilm is not available in most of the reported cases. It is well documented that for biofilm formation flagella and extracellular polysaccharides (EPS) play crucial roles in all biofilm-forming bacterial strains, besides other biochemical/biological factors (Lin, Santos, Kontur, Donohue, Weibel 2015; Sauer, Camper, Ehrlich, Costerton, Davies, 2002; Tsuneda, Aikawa, Hayashi, Yuasa, Hirata, 2003).The cells of *Rhodopseudomonas sp* are known to be single-flagellated (monotrichous) which helps in the motility as well as attachment to substratum surface and they also secrete EPS in biofilm assemblages (Lin et al., 2015; Wilkinson, Chacko, Venien-Bryan, Wadhams, Armitage, 2011). From a comparative study between a wild type (flagellated) and its non-flagellated mutant, it was experimentally observed that presence of flagella was essential for surface adhesion and biofilm formation in PNSB

(Wilkinson et al., 2011). The rod-shaped morphology of PNSB cells advantageously facilitates larger contact area and tighter attachment of initial cells onto the substratum than sphere-shaped bacterial cells (Lin et al., 2015). The length and diameter of each *Rhodopseudomonas sp* cell was taken to be 1.4μm and 0.5μm respectively, as apparent from the transmission electron microscope images provided in a recent literature (Jung, Jung, Kim, Ahn, Park, 1999).

In the present system, biofilm formation was proposed to be initiated by the longitudinal attachment of the *Rhodopseudomonas sp* cells on the surface of glass plates forming the first layer of biofilm. Subsequent layers of biofilm were formed by proliferation of cells in attached phase. The mechanism could be justified by the already reported tendency of attached growth of subclass-3 of α-proteobacteria to which *Rhodopsuedomonas sp* belong (Conlan, Lawrence, McCue, 2005; Pechter, Gallagher, Pyles, Manoil, Harwood, 2015). It is evident from the literature that in presence of light, the GGDEF domain of bacteriophytochrome, BphG1 possessing diguanylatecyclase activity, responsible for the synthesis of cyclic di-GMP [bis-(3'-5')-cyclic di-GMP], in PNSB is triggered (Tarutina, Ryjenkov, Gomelsky 2006; Ryan, Fouhy, Lucey, Dow 2006). Moreover, high concentrations of intracellular c-di-GMP promote bacterial biofilm formation (Ryan et al., 2006). Since all FBPPBRs are sufficiently illuminated, the high level of c-di-GMP is therefore ensured facilitating attached growth of PNSB. Using the same justification, the reversibility of attachment of *Rhodopseudomonas sp* in the early stage of biofilm formation, reported in case of *Pseudomonas aeruginosa* (Sauer et al., 2002), has been disregarded. It is assumed that after the irreversible attachment, the biofilm of *Rhodopseudomonas sp* goes through a single proliferation stage governed by the Las quorum sensing mechanism until a maturation stage is reached at a biofilm thickness of 100 mm. As evident from the reported studies on bacterial biofilm, the maturation stage is followed by a

177 dispersal stage when the biofilm is detached from the substratum and the cells start growing in
178 suspension until another cycle of biofilm formation is commenced (Davies et al., 1998). The
179 proposed mechanism of formation of biofilm of *Rhodopseudomonas sp* has been depicted in
180 Figure 2 showing sequential stages.

181 **2. Materials and methods**

182 **2.1. Materials**

183 The following materials were used for the present study:

184 *2.1.1. Microorganism*

185 *Rhodopseudomonas sp* (MTCC 8756) was obtained from MTCC, Chandigarh, India.

186 *2.1.2. Equipments and Instruments*

187 Digital weighing machine (Sartorius), autoclave (Gurpreet Engineering Works), Hot air Oven,
188 BOD incubator shaker (G. B. Enterprises, Kolkata, India) fitted with 4 CFL lights, Table Top
189 Centrifuge (Spinwin,India), Laminar air flow bench, Luxmeter(Lutron, Taiwan), Gas
190 Chromatography and UV-Vis spectrophotometer (, India) were used.

191 **2.2. Methods**

192 *2.2.1. Growth medium for pre-adaptation*

193 All chemicals were of analytical grade (MerckSpecialties Private Limited, India) and were used
194 without any further purification. Phototrophic bacteria *Rhodopseudomonas sp*was pre-adapted to
195 modified Biebl and Pfennig medium (g dm^{-3}): Yeast extract 0.3, ammonium acetate 0.5,
196 $KHPO_4$0.5, K_2HPO_4 0.5, $MgSO_4.7H_2O$ 0.3, NaCl 0.3, $CaCl_2.2H_2O$ 0.05, L-cysteinihydrochloride

197 0.4, L-malic acid 1, sodium succinate 1, dextrose 5, vitamin B_{12} solution (0.01% w/v) 0.4 ml/l,
198 ferric citrate solution (0.01% w/v) 5 ml/l, agar (2%) and trace element solution SL-6 1 ml/l. The
199 trace element solution constituted (g dm^{-3}): $ZnSO_4.7H_2O$ 0.05, $MnCl_2.4H_2O$ 0.03, H_3BO_3 0.3,
200 $CoCl_2.6H_2O$ 0.2, $CuCl_2.2H_2O$ 0.01, $NiCl_2.6H_2O$ 0.02, $Na_2MoO_4.2H_2O$ 0.03. Sterility was
201 maintained by autoclaving at 2.04 kg/cm^2, 121℃ for 15 minutes. The light intensity was
202 maintained at 64W/m^2 for the growth experiments.

203 *2.2.2. Batch mode experiments for growth kinetics*

204 Batch mode experiments in 50ml Erlenmeyer flasks were performed to determine the growth
205 kinetics of pre-adapted *Rhodopseudomonas sp*. by varying the concentration (1-10g/L) of malic
206 acid in the modified Biebl and Pfennig medium. The temperature and pH was maintained at 37℃
207 and 6.5-7.0 respectively.After inoculating the medium with pre-adapted culture of
208 *Rhodopseudomonas sp*., the head space was purged with Argon to create an oxygen free
209 environment. For each initial malic acid concentration after every four-hour time interval
210 samples were collected from the conical flasks of respective hour and analysed by the
211 conventional gravimetric method to determine the biomass concentration at particular time. The
212 collected samples were centrifuged for 30mins at 10000 rpm in a table top centrifuge, in 1.5 ml
213 pre weighed Eppendorf tubes.
214 After centrifugation, the supernatant was discarded and the pellet was allowed to dry for
215 overnight at 105℃ in hot air oven. The eppendorf with dried pellet was weighed and subtracted
216 by the weight of empty Eppendorf tubes. Therefore, the amount of biomass present in 1.5ml of
217 sample and the biomass concentration in the sample was calculated.

218 *2.2.3. Determination of Growth Kinetics*

219 On obtaining the biomass concentration at every fourth interval for corresponding DL malic acid
220 concentration, growth curves of cell concentration vs. time was plotted. From these growth
221 curves the growth kinetic parameters were determined by fitting using Monod growth model
222 which is represented as follows:

223 $$\mu = \frac{\mu_{\max} C_S}{K_S + C_S}$$

224 The kinetic parameters (μ_{max} and K_S) were calculated from the initial specific growth rate (μ) for
225 each corresponding malic acid concentration. From the double reciprocal or Lineweaver-Burk
226 (plot not shown) the values of μ_{max} and K_S were calculated and have been tabulated in Table 1.

227 **3. MATHEMATICAL ANALYSIS**

228 *3.1. Model of Batch Reactor for Biofilm Development*

229 The batch reactor, schematically represented in Figure 3, is proposed for the development of
230 biofilm, prior to its utilization in the flat plate bioreactors.

231 The following assumptions have been made for the development of the mathematical model.

232 1. All the operations are considered to be under isothermal conditions since the heat effect
233 of biochemical reactions is low.
234 2. The growth of PNSB biomass is in exponential phase and is balanced.
235 3. The utilization of substrate for the cell maintenance is negligible.
236 4. Both flagellar movement and EPS synthesis requires energy expenditure in form of ATP,
237 which is produced from the metabolic utilization of the carbon substrate for PNSB
238 biomass growth. Due to this, no hydrogen is produced during the early and
239 developmental stages of biofilm, until the more mature biofilm is used in the FPPBR
240 reactor.

5. The hydrogen produced in the photo fermentative process is a growth associated product.
6. Cells are attached longitudinally to the glass surface to form a monolayer as soon as they are formed in suspension. Afterwards the cells are attached to those forming the first layer and so on to develop multi-layered biofilm.
7. The biofilm is developed uniformly on both faces of the glass plate.
8. Biofilm development on the reactor walls has been neglected which can justified by the fact that the cells get attached only on the surface-modified glass plates.
9. The planktonic dispersal of attached cells through up-regulation of quorum sensing or other mechanisms has been neglected.

The mass balance equations for the substrate, biomass, biofilm thickness and biomass in biofilm have been provided in Table 2.

In order to derive a correlation between the biomass concentration due to planktonic growth and the thickness of the biofilm developed through attachment on the glass surface at any instant, the following equation has been used. It was assumed that a gram of biomass contains 10^{12} cells (Davis & Ginsberg, 1973).

$$Number\ of\ layers\ formed\ (N_L) = \frac{C_X V * 10^{12} * a}{2 * S}$$

$$Thickness\ of\ biofilm\ (Th) = N_L * d$$

where,

C_X=Concentration of the biomass at a given time instant.

V=Working Volume of the culture medium

S= Surface area of the glass plate.

d= Diameter of a single *Rhodopseudomonas sp*cell.

a = Surface area covered by each attached PNSB cell.

Therefore,

$$\frac{d(Th)}{dt} = p * \frac{dC_X}{dt} \; where, p = \frac{V * 10^{12} * a * d}{2 * S}$$

$$V = V_a + V_b$$

where, V_a = volume of the abiotic phase

and V_b = volume of the biotic phase

$$= S * Th$$

Since it is assumed that all microbial cells in the medium form biofilm and undergo planktonic growth, the concentration of biomass in the biofilm, C_{Xb} at any time t>0 in the batch reactor is as follows:

$$C_{Xb} = \frac{C_X V}{V_b}$$

C_{Xb}, the concentration of biomass in the biofilm formed, can be expressed in terms of cell number (N) concentration as shown below:

$$N = C_{Xb} * 10^{12} \; cells / L = C_{Xb} * 10^{6} \; cells / \mu L$$

Therefore, in terms of the concentration of biomass in the biofilm

$$Number \; of \; layers \; formed \; (N_L) = \frac{C_{Xb} V_b * 10^{12} * a}{2 * S}$$

$$\frac{dC_{Xb}}{dt} = \mu C_{Xb}$$

The initial conditions are as follows:

$$For \; t = 0 : C_S = C_{S0} \; ; C_X = C_{X0} \; ; C_{Xb} = 0 \; and \; Th = 0 \qquad (1)$$

The differential equations listed in Table 2 have been solved simultaneously by employing the ode45 solver of MATLAB software using the initial conditions represented by Equation 1. The values of all input variables and model constants are provided in Table 1.

3.2. Model for Continuous Circular and Rectangular FPPBR

The flat plate circular PBR along with differential sections has been schematically represented in Figure 4. For formulating the system equations for the circular biofilm FPPBR, a couple of assumptions in addition to the ones used in case of the batch reactor for biofilm development have been made:

1. The fluid flow of the culture medium inside the reactor is in the ideal plug mode, i.e., all axial and radial dispersions are negligible.
2. The system operates under steady state condition with respect to the biofilm thickness, i.e., there is no variation of the biofilm thickness with time at any spatial coordinate.

The mass balance equations for the substrate, product, biofilm thickness and biomass in biofilm have been provided in Table 3.

The two dimensional variation of the species concentration has been simplified to a 1-D model by replacing the angle (θ) subtended at the centre of the circular plate of radius 'R' as function of the radial position 'r' as follows

$$\theta = \sin^{-1}(\frac{r}{R})$$

The material balance equation for biomass over the differential elemental strip spanning between 'r' and 'r+Δr' on the circular plate, as shown in Figure 4(b), is as follows:

$$\frac{u}{r}\frac{d(rC_{Xb})}{dr} + \frac{u}{r} * R\cos\theta\frac{dC_{Xb}}{dr} = \mu C_{Xb}$$

where, u is the superficial velocity at which the culture medium flows through the circular plate bioreactor.

$$\mu = \left(\frac{\mu_m C_S}{K_S + C_S}\right) * \frac{I}{K_{XI} + I + K_I I^2}$$

Using the correlation between 'θ' and 'r', the above equation reduces to the following form:

$$\frac{dC_{Xb}}{dr} = \frac{r}{u} \frac{(\mu - u) C_{Xb}}{r + R\cos(\sin^{-1}(\frac{r}{R}))}$$

The corresponding equations for the biofilm thickness, substrate and product concentration are as follows:

$$\frac{d(Th)}{dr} = p * \frac{dC_{Xb}}{dr}$$

$$\frac{dC_S}{dr} = -\frac{1}{Y_{X/S}} \frac{dC_{Xb}}{dr}$$

$$\frac{dC_P}{dr} = Y_{P/X} \frac{dC_{Xb}}{dr} * \frac{I}{K_{PI} + I + K_{pI} I^2}$$

The boundary conditions are as follows: at all radial positions with r=R:

$$C_S = C_{S0}\,; C_{Xb} = C_{Xbf}\,; C_P = 0 \; and \; Th = Th_f \qquad (2)$$

where, Th_f is the final thickness of biofilm and C_{Xbf} is the final biomass concentration in the biofilm achieved in the batch reactor for biofilm development. The differential equations listed in Table 3for circular FPPBR have been solved simultaneously by employing the ode45 solver of MATLAB software using the boundary conditions represented by Equation 2 to obtain the spatial distribution of the species concentration inside the bioreactor.

The rectangular FPPBR along with differential sections has been schematically represented in Figure 5(a). For the case of the rectangular flat plate PBR, the model has been developed with

322 the same assumptions as in the case of the circular plate one. Referring to Figure 5(b), the
323 differential equations representing the axial gradients of substrate, product, biofilm thickness and
324 biomass in biofilm have been provided in Table 3.

325 The material balance equation for the cellular mass, over the differential elemental as shown in
326 Figure 5(b) in between 'x' and 'x+Δx' on the rectangular plate yields:

327 $$u\left(\frac{\delta C_{Xb}}{\delta x} + \varepsilon \frac{\delta C_{Xb}}{\delta y}\right) = \mu C_{Xb}$$

328 where, ε is the fraction of the x-directional velocity which gets transferred in the y-direction.

329 Converting this 2-D model to a 1-D model by expressing 'y' as a function of 'x' as follows:

330 $y = \frac{S}{x}$ where 'S' is the surface area of the plate. Replacing it in the above equation and
331 simplifying to get the final form:

332 $$\frac{dC_{Xb}}{dx} = \frac{\mu C_{Xb}}{u * \left(1 - \frac{x^2 \varepsilon}{S}\right)}$$

333 The corresponding equations for the biofilm thickness, substrate and product concentration are as
334 follows:

335 $$\frac{d(Th)}{dx} = p * \frac{dC_{Xb}}{dx}$$

336 $$\frac{dC_S}{dx} = -\frac{1}{Y_{X/S}} \frac{dC_{Xb}}{dx}$$

337 $$\frac{dC_P}{dx} = Y_{P/X} \frac{dC_{Xb}}{dx} * \frac{I}{K_{PI} + I + K_{pI} I^2}$$

338 The boundary conditions are as follows; At all axial positions with x=0:

339 $C_S = C_{S0}\,; C_{Xb} = C_{Xbf}\,; C_P = 0 \, and \;\; Th = Th_f$ (3)

340 Similar to the circular plate, the equations listed in Table 3 for rectangular FPPBR have been
341 solved simultaneously by employing the ode45 solver of MATLAB software using the boundary
342 conditions represented by Equation 3 to get the axial distribution of the concentrations of the
343 different species inside the rectangular plate.

344 **4. Results and discussions**

345 *4.1. Flow Pattern inside the Biofilm of Rhodopseudomonas sp*

346 The flow pattern of the substrate medium inside the biofilm of *Rhodopseudomonas sp* in an
347 FPPBR was modeled using COMSOL Multiphysics. The flow inside the biofilm was considered
348 to belaminar flow in porous matrix and the malic acid containing medium was approximated as
349 transport of dilute species. Also, the effect of diffusion (the value of diffusion coefficient was
350 taken to be $1.68*10^{-9}$ m^2 h^{-1}) (Liao et al., 2012) was considered while defining the transport
351 equations for the system under consideration. Figure 6 showed the variation in flow pattern with
352 non-dimensional spatial dimensions and suggested that the assumption of neglecting the
353 diffusive flow components while formulating the system equations for circular and rectangular
354 FPPBR was justified since the flow pattern showed minimal change upon incorporating the
355 diffusion effects.

356 *4.2. Model Predictions for Batch FPPBRs*

357 *4.2.1. Time History of Substrate Concentration*

358 Figure 7 shows the pattern of dynamic variation of concentration of malic acid at different values
359 of its initial concentration in the batch reactors of circular and rectangular cross sections, used for
360 the development of biofilm. It is worth mentioning that rectangular hyperbolic pattern of

361 declining time histories of substrate is following in the entire initial concentration range. As per
362 expectation, the concentration profiles of malic acid corresponding to higher initial values
363 always lie above those obtained at lower ones. The similar declining trends of the substrate
364 consumption profiles, as predicted by the model, have also been observed by previous research
365 groups during their studies on hydrogen production in batch reactors using different *Rhodobacter*
366 species (Ozgur et al., 2012; Nath, Kumar, Das, 2005; Basak & Das, 2009; Kapdan, Kargi,
367 Oztekin, Argun, 2009). However, the information on the substrate concentration profile during
368 the development of biofilm of *Rhodobacter* species in batch system is not available in the
369 literature.

370 *4.3. Attached Cell Growth*

371 *4.3.1. Cell Number Concentration of Biomass in the Biofilm*

372 An attempt has been made to propose the mechanism of attached growth of *Rhodopseudomonas*
373 *sp* to provide a better understanding of the dynamics of biomass layer (biofilm) formation. The
374 change in the cell number concentration of biomass in the biofilm during the microbial growth
375 for different initial concentration of malic acid is shown in Figure 8. The number density of cells
376 gradually increases upon increasing the initial substrate concentration because the inhibitory
377 effect of substrate, decaying rate of cells as well as the shadowing effect of light at high
378 concentrations of bacterial biomass are assumed to be negligible. Similar dynamic behavior of
379 suspended cell concentration has been reported for studies involving immobilized *Rhodobacter*
380 *sphaeroides* in a rocking photobioreactor (Gilbert, Ray, Das, 2011). The cell density (log
381 N=8.53-9.4) of *Rhodopseudomonas sp* in the biofilm is comparable to that of *Escherichia coli*

382 and *Staphylococcus aureus* (both are around 10^8 colony forming unit/ml) (Kirby, Garner, Levin,
383 2012).

384 *4.3.2. Thickening of Biofilm*

385 Next, the effect of time on the thickness of the biofilm formed has been examined as shown in
386 Figure 9. It has been observed that the biofilm thickness gradually increases with time and
387 saturates after a certain interval of time. The point of saturation also marked the time instant
388 when the replenishment of substrate from external sources is required. The biofilm thickness
389 varies between 11.52μm and 55.7μm as the initial malic acid concentration is varied from 1g/l to
390 10g/l. It can be said from a previous work (Sauer et al., 2002) employing *Pseudomonas*
391 *aeruginosa*, that the biofilm produced in this case attained maturation and the number of layers
392 subsequently increased.

393 *4.3.3. Biofilm Thickness-Specific Growth Rate Phase Plane Diagrams*

394 The variation of the specific growth rate at the top surface of the growing biofilm with biofilm
395 thickness has also been studied as shown in Figure 10. From the analysis of the figure, it is clear
396 that the specific growth rate remains constant with the increase of biofilm thickness up to a
397 critical value of the latter beyond which it falls to zero. The critical biofilm thickness signifies
398 the complete exhaustion of the substrate in the reactor and hence the stagnation of further
399 attached growth of cells. The biofilm could have been grown further if more substrate were
400 present in the bioreactor.

401 *4.4. Model Predictions for Continuous FPPBRs*

402 *4.4.1. Spatial distribution*

Hydrogen production has been modeled in a circular plate reactor of diameter 100mm and thickness 6mm. Figure 11 illustrates the performance of the circular plate PBR with respect to the hydrogen production and cell growth with a constant photon concentration of 320μmoles/m^2/s. A gradual increase in the hydrogen production is observed from the point of entry into the reactor after which it reaches an almost saturation level of 0.3390 g/l at r=0.07m. The variations of the biomass concentration and the biofilm thickness follow expected patterns with the latter saturating at 38μm. The substrate concentration undergoes gradual decline from the point of entry since the PNSB starts to utilize the malic acid as carbon substrate for its growth and hydrogen production. The point where the substrate gets exhausted coincides with the points where the hydrogen and biomass profiles reach saturation indicating no more substrate is present in the system for the microbial uptake and provides an indirect proof of the conservation of mass in the reactor. This result is also pertinent to the assumption stating hydrogen as a growth associated product.

Figure 12 shows the performance of the rectangular plate PBR configuration in presence of light (320μmoles/m^2/s). The amount of hydrogen produced (0.1210 g/l) using this reactor configuration is found to be less than its circular counterpart. The cause of such a decline in the hydrogen production might be due to the fact that in case of the circular reactor the culture medium gets exposed to a small arc of the circular area which progressively goes on increasing. This allows the medium enough residence time as well as accessible surface area to enhance the hydrogen production. On the other hand, for the rectangular plate the culture medium gets exposed to the entire available area as soon as it enters the reactor thereby reducing the residence time and hence there is a fall in the hydrogen production.

4.5. Model Critique

Therefore, in summary, the models proposed in this work provide valuable insight to the development of biofilm of *Rhodopseudomonas sp* in a batch reactor. It can successfully predict the substrate consumption as well as the biofilm dynamics. The models can also quantify the cell density of the PNSB cells present in the biofilm. Although the predictions of the model are in good agreement with available literature data on similar research studies, there are scopes for the refinement of the models by the incorporation of exact relationship between suspended and attached microbial cells, disintegrated biofilm formation and real attachment of the PNSB cells having different orientations on the surface of the immobilization matrix in the reactor. Since the usage of phototrophic consortium (Montiel-Corona, Revah, Morales, 2015) for H_2 production is also in trend, mathematical interpretation of mixed culture interaction, as proposed in a pioneering research article (Tang & Liu, 2017), can also be incorporated in the model.

Conclusion

It is of paramount importance to study the growth dynamics of PNSB cell population in order to have a better understanding of the biohydrogen production process and computational modeling is an effective way to design bioreactors for such bioprocess applications. The developmental stage in a batch reactor as well as the hydrogen production stage of PNSB in an immobilized continuous FPPBR have been designed and simulated in this study. The simulated value of biofilm thickness ranges from 12-56μm depending upon the quantity of substrate initially charged in the batch reactor used for biofilm development. Finally, the effect of geometry of the PBR on the hydrogen production has been studied taking into account a circular and a rectangular FPPBR. It has been observed that there is a 64.3% decrease in hydrogen production in the rectangular FPPBR as compared to the circular one of same surface area coverage by biofilm. In summary, our results show promising potential for the development of immobilized

cell FPPBRs for hydrogen production by establishing a synergistic relation among traditional chemical, biochemical and bioprocess engineering principles and it is expected that the results will help in designing more efficient FPPBRs for hydrogen production using PNSB cells.

Acknowledgements

Authors gratefully acknowledge their parent institution Jadavpur University for providing technical and infrastructural facilities for the conduction of this research work.

Nomenclature

A	Surface area covered by each attached *Rhodopseudomonas sp* cell (m^2)
C_P	Concentration of Product (Hydrogen) (g L^{-1})
C_S	Concentration of Substrate (Malic Acid) (g L^{-1})
C_{S0}	Initial Concentration of Substrate (Malic Acid) (g L^{-1})
C_X	Concentration of Biomass (*Rhodopseudomonas sp*) (g L^{-1})
C_{X0}	Initial Concentration of Biomass (g L^{-1})
C_{Xb}	Concentration of Biomass In The Biofilm (g L^{-1})
C_{Xbf}	Concentration of Biomass In The Biofilm achieved in the Batch Reactor (g L^{-1})
D	Diameter of a single *Rhodopseudomonas sp* cell (μm)
K_S	Half-SubstrateSaturation Constant (g L^{-1})
N	Cell Number Concentration (cells μL^{-1})
N_L	Number of Biofilm Layers
R	Radial Distance from the edge of the Circular Plate Photobioreactor (m)
R	Radius of the Circular Flat Plate Photobioreactor (m)
S	Surface Area of Flat Plate Photobioreactor (m^2)
Th	Biofilm Thickness (μm)
Th_f	Biofilm Thickness achieved in the Batch Reactor (μm)
U	Superficial Velocity of Culture Medium (m s^{-1})
V	Working Volume of Culture Medium (L)
V_a	Volume of Abiotic Phase (L)
V_b	Volume of Biotic Phase (L)
X	Axial Distance from the edge of the Rectangular Plate Photobioreactor (m)
$Y_{P/X}$	Yield of Product in terms of Biomass (g Product/g Biomass)

$Y_{X/S}$	Biomass Yield Coefficient (g Biomass/g Substrate)

REFERENCES

1. Skjanes, K., Knutsen, G., Kallqvist, T., & Lindblad, P. (2008). H_2 production from marine and freshwater species of green algae during sulphur deprivation and considerations for bioreactor design. *International Journal of Hydrogen Energy* 33, 511-521.
2. Berberoglu, H., Yin, J., & Pilon, L. (2007). Light transfer in bubble sparged photobioreactors for H_2 production and CO_2 mitigation. *International Journal of Hydrogen Energy* 32, 2273-2285.
3. Molina, G. E., Fernandez, J., Acien, F. G., & Chisti, Y. (2001). Tubular photobioreactor design for algal cultures. *Journal of Biotechnology* 92, 113-131.
4. Dasgupta, C. N., Gilbert, J. J., Lindblad, P., Heidorn, T., Borgvang, S. A., Skjanes, K., & Das, D. (2010). Recent trends on the development of photobiological processes and photobioreactors for the improvement of hydrogen production. *International Journal of Hydrogen Energy* 35, 10218-10238.
5. Xu, Z., Dapeng, L., Yiping, Z., Xiaoyan, Z., Zhaoling, C., Wei, C., & Fan, O. (2002). Comparison of photobioreactors for cultivation of *Undaria pinnatifida* gametophytes. *Biotechnology Letters* 24, 1499-1503.
6. Janssen, M., Tramper, J., Mur, L. R. & Wijffels, R. H. (2003). Enclosed outdoor photobioreactors: light regime, photosynthetic efficiency, scale-up and future prospects. *Biotechnology and Bioengineering* 81, 193-210.

7. Pradhan, L., Bhattacharjee, V., Mitra, R., Bhattacharya, I. & Chowdhury, R. (2015). Biosequestration of CO_2 using power plant algae (*Rhizoclonium hieroglyphicum* JUCHE2) in a Flat Plate Photobio-Bubble-Reactor - Experimental and modelling. *Chemical Engineering Journal* 275,381-390.
8. Miron, A. S., Gomez, A. C., Camacho, F. G., Molina, G. E., & Chisti, Y. (1999) Comparative evaluation of compact photobioreactors for large-scale monoculture of microalgae. *Journal of Biotechnology* 70, 249-270.
9. Lehr, F., & Posten, C. (2009). Closed photo-bioreactors as tools for biofuel production. *Current Opinions in Biotechnology* 20, 280-285.
10. Richmond, A. (2000) Microalgal biotechnology at the turn of the millennium: a personal view. *Journal of Applied Phycology* 12, 441-451.
11. Hu, Q., Gutermann, H., & Richmond, A. (1996). A flat inclined modular photobioreactor for the outdoor mass cultivation of photoautotrophs. *Biotechnology and Bioengineering* 51, 51-60.
12. Akkerman, I., Janssen, M., Rocha, J., & Wijffels, R. H. (2002). Photobiological hydrogen production: photochemical efficiency and bioreactor design. *International Journal of Hydrogen Energy* 27, 1195-1208.
13. Gross, M., & Wen, Z. (2014). Yearlong evaluation of performance and durability of a pilot scale Revolving Algal Biofilm (RAB) cultivation system. *Bioresource Technology* 171,50-58.
14. Irving, T. E. & Allen, D. G. (2011). Species and material considerations in the formation and development of microalgal biofilms. *Applied Microbiology Biotechnology* 92,283-294.

15. Zhuang, L. L., Hu, H. Y., Wu, Y. H., Wang, T., & Zhang, T. Y. (2014). A novel suspended-solid phase photobioreactor to improve biomass production and separation of microalgae. *Bioresource Technology* 153, 399-402.
16. Genin, S. N., Aitchison, J. S. & Allen, D. G. (2015). Novel waveguide reactor design for enhancing algal biofilm growth. *Algal Research* 12, 529-538.
17. Johnson, M. B., & Wen, Z. (2010). Development of an attached microalgal growth system for biofuel production. *Applied Microbiology Biotechnology* 85, 525–534.
18. Liu, T., Wang, J., Hu, Q., Cheng, P., Ji, B., Liu, J., Chen, Y., Zhang, W., Chen, X., Chen, L., Gao, L., Ji, C., & Wang, H. (2013). Attached cultivation technology of microalgae for efficient biomass feedstock production. *Bioresource Technology* 127, 216–222.
19. Tamburic, B., Zemichael, F. W., Crudge, P., Maitland, G. C., & Hellgardt, K. (2011). Design of a novel flat-plate photobioreactor system for green algal hydrogen production. *International Journal of Hydrogen Energy* 36, 6578-6591.
20. Christenson, L. B. & Sims, R. C. (2012). Rotating algal biofilm reactor and spool harvester for wastewater treatment with biofuels by-products. *Biotechnology and Bioengineering* 109,1674-1684.
21. Tao, Q., Gao, F., Qian, C. Y., Guo, X. Z., Zheng, Z., & Yang, Z. H. (2017). Enhanced biomass/biofuel production and nutrient removal in an algal biofilm airlift photobioreactor. *Algal Research* 21, 9–15.
22. Li, L., Suwanate, S. & Visvanathan, C. (2017) Performance evaluation of attached growth membrane bioreactor for treating polluted surface water. *Bioresource Technology* 240, 3-8.

523 23. Ozkan, A., Kinney, K., Katz, L., & Berberoglu, H. (2012). Reduction of water and energy
524 requirement of algae cultivation using an algae biofilm photobioreactor *Bioresource*
525 *Technology* 114, 542–548.
526 24. He, Y., Chen, L., Zhou, Y., Chen, H., Zhou, X., Cai, F., Huang, J., Wang, M., Chena, B.,
527 & Guo, Z. (2016). Analysis and model delineation of marine microalgae growth and lipid
528 accumulation in flat-plate photobioreactor. *Biochemical Engineering Journal* 111:108-
529 116.
530 25. Kandilian, R., Tsao, T. C.,5 & Pilon, L. (2014). Control of incident irradiance on a batch
531 operated flat-plate photobioreactor. *Chemical Engineering Science* 119, 99–108.
532 26. Zhang, Q. H., Wu, X., Xue, S. Z., Wang, Z. H., Yan, C. H. & Cong, W. (2013).
533 Hydrodynamic Characteristics and Microalgae Cultivation in a Novel Flat-Plate
534 Photobioreactor. *Biotechnology Progress* 29, 127-134.
535 27. Koller, A. P., Löwe, H., Schmid, V., Mundt, S., & Weuster-Botz, D. (2017). Model-
536 supported phototrophic growth studies with *Scenedesmus obtusiusculus* in a flat-plate
537 photobioreactor. *Biotechnology and Bioengineering* 114, 308–320.
538 28. Ghosh, S., Dairkee, U. K., Chowdhury, R., & Bhattacharya, P. (2016). Hydrogen from
539 food processing wastes via photofermentation using Purple Non-sulfur Bacteria (PNSB)
540 – A review. *Energy Conversion and Management* 141, 299-314.
541 29. Wu, T. Y., Hay, J. X. W., Kong, L. B., Juan, J. C., & Jahim, J. M. (2012). Recent
542 advances in reuse of waste material as substrate to produce Biohydrogen by purple non-
543 sulfur (PNS) bacteria. *Renewable and Sustainable Energy Reviews* 16, 3117-3122.

30. Adessi, A., Torzillo, G., Baccetti, E., & De Philippis, R. (2012). Sustained outdoor H_2 production with *Rhodopseudomonas palustris* cultures in a 50 L tubular photobioreactor. *International Journal of Hydrogen Energy* 37, 8840-8849.
31. Zagrodnik, R., Thiel, M., Seifert, K., Włodarczak, M., & Łaniecki, M. (2013). Application of immobilized *Rhodobacter sphaeroides* bacteria in hydrogen generation process under semi-continuous conditions. *International Journal of Hydrogen Energy* 38, 7632-7639.
32. Zagrodnik, R., Seifert, K., Stodolny, M., & Laniecki, M. (2015). Continuous photofermentative production of hydrogen by immobilized *Rhodobacter sphaeroides* O.U.001. *International Journal of Hydrogen Energy* 40, 5062-5073.
33. Tang, Y., & Liu, H. (2017). Modeling Multidimensional and Multispecies Biofilms in Porous Media. *Biotechnology and Bioengineering* 114, 1679-1687.
34. Ward, J., Wattis, J., Jabbari, S., Siggers, J., Kabayashi, R., Armitage, J., Godfrey, S., & Packer, H. (2005). Modelling the development and formation of biofilms. http://www.maths-in-medicine.org/uk/2005/biofilms/
35. Liao, Q., Wang, Y. J., Wang, Y. Z., Chen, R., Zhu, X., Pu, Y. K., & Lee, D. J. (2012). Two-dimension mathematical modeling of photosynthetic bacterial biofilm growth and formation. *International Journal of Hydrogen Energy* 37, 15607-15615.
36. Xie, G. J., Liu, B. F., Ding, J., Xing, D. F., Ren, H. Y., Guo, W. Q., & Ren, N. Q. (2012). Enhanced photo-H_2 production by *Rhodopseudomonas faecalis* RLD-53 immobilization on activated carbon fibers. *Biomass Bioenergy* 44,122-129.

565 37. Zhang, C., Zhu, X., Liao, Q., Wang, Y., Li, J., Ding, Y., & Wang, H. (2010).
566 Performance of a groove-type photobioreactor for hydrogen production by immobilized
567 photosynthetic bacteria. *International Journal of Hydrogen Energy* 35, 5284-5292.
568 38. Tian, X., Liao, Q., Liu, W., Wang, Y. Z., Zhu, X., Li, J., & Wang, H. (2009). Photo-
569 hydrogen production rate of a PVA-boric acid gel granule containing immobilized
570 photosynthetic bacteria cells. *International Journal of Hydrogen Energy* 34, 4708-4717.
571 39. Lin, T. Y., Santos, T. M. A., Kontur, W. S., Donohue, T. J., & Weibel, D. B. (2015). A
572 Cardiolipin-Deficient Mutant of *Rhodobacter sphaeroides* Has an Altered Cell Shape and
573 Is Impaired in Biofilm Formation. *Journal of Bacteriology* 197, 3446-3455.
574 40. Sauer, K., Camper, A. K., Ehrlich, G. D., Costerton, J. W. & Davies, D. G. (2002).
575 *Pseudomonas aeruginosa* Displays Multiple Phenotypes during Development as a
576 Biofilm. *Journal of Bacteriology* 184, 1140–1154.
577 41. Tsuneda, S., Aikawa, H., Hayashi, H., Yuasa, A., & Hirata, A. (2003). Extracellular
578 polymeric substances responsible for bacterial adhesion onto solid surface. *FEMS*
579 *Microbiology Letters* 223, 287-292.
580 42. Wilkinson, D. A., Chacko, S. J., Venien-Bryan, C., Wadhams, G. H., & Armitage, J. P.
581 (2011). Regulation of Flagellum Number by FliA and FlgM and Role in Biofilm
582 Formation by *Rhodobacter sphaeroides*. *Journal of Bacteriology* 193, 4010-4014.
583 43. Jung, G. Y., Jung, H. O., Kim, J. R., Ahn, Y., & Park, S. (1999). Isolation and
584 characterization of *Rhodopseudomonas palustris* P4 which utilizes CO with the
585 production of H_2. *Biotechnology Letters* 21, 525–529.

586 44. Conlan, S., Lawrence, C., & McCue, L. A. (2005). *Rhodopseudomonas palustris*
587 Regulons Detected by Cross-Species Analysis of Alphaproteobacterial Genomes. *Applied*
588 *Environmental Microbiology* 71, 7442-7452.
589 45. Pechter, K. B., Gallagher, L., Pyles, H., Manoil, C. S., & Harwood, C. S. (2015).
590 Essential Genome of the Metabolically Versatile Alphaproteobacterium
591 *Rhodopseudomonas palustris*. *Journal of* Bacteriology 198, 867-876.
592 46. Tarutina, M., Ryjenkov, D. A. & Gomelsky, M. (2006). An Unorthodox
593 Bacteriophytochrome from *Rhodobacter sphaeroides* Involved in Turnover of the Second
594 Messenger c-di-GMP. *Journal of Biological Chemistry* 281, 34751-34758.
595 47. Ryan, R. P., Fouhy, Y., Lucey, J. F., & Dow, J. M. (2006). Cyclic Di-GMP Signaling in
596 Bacteria: Recent Advances and New Puzzles. *Journal of Bacteriology* 188, 8327-8334.
597 48. Davies, D. G., Parsek, M. R., Pearson, J. P., Iglewski, B. H., Costerton, J. W., &
598 Greenberg, E. P. (1998). The involvement of cell-to-cell signals in the development of a
599 bacterial biofilm. *Science* **280**, 295–298.
600 49. Uyara, B., Eroglu, I., Yucel, M., Gunduz, U., & Turker, L. (2007). Effect of light
601 intensity, wavelength and illumination protocol on hydrogen production in
602 photobioreactors. *International Journal of Hydrogen Energy* 32, 4670 – 4677.
603 50. Gadhamshetty, V., Sukumaran, A., Nirmalakhandan, N., & Myint, M. T. (2008).
604 Photofermentation of malate for biohydrogen production-A modeling approach.
605 *International Journal of Hydrogen Energy* 33, 2138-2146.
606 51. Monod, J. (1942). Recherchesur la croissance des cultures bactériennes (Thèse
607 Doctoratès Sciences Naturelles). Paris: Hermann.

608 52. Don, M. M., & Shoparwe, N. F. (2010). Kinetics of hyaluronic acid production by
609 *Streptococcus zooepidemicus* considering the effect of glucose. *Biochemical Engineering*
610 *Journal* 49, 95-103.
611 53. Gadhe, A., Sonawane, S. S., & Varma, M. N. (2013). Optimization of conditions for
612 hydrogen production from complex dairy wastewater by anaerobic sludge using
613 desirability function approach. *International Journal of Hydrogen Energy* 38, 6607-6617.
614 54. Davis, D., & Ginsberg, E. (1973). Bacterial Physiology: Microbiology (2nd Edition).
615 Maryland: Harper and Row.
616 55. Ozgur, E., Uyar, B., Ozturk, Y., Yucel, M., Gunduz, U., & Eroglu, I. (2010).
617 Biohydrogen production by *Rhodobacter capsulatus* on acetate at fluctuating
618 temperatures. *Resources, Conservation and Recycling* 54, 310–314.
619 56. Nath, K., Kumar, A., & Das, D. (2005). Hydrogen production by *Rhodobacter*
620 *sphaeroides* strain O.U.001 using spent media of *Enterobacter cloacae* strain DM11.
621 *Applied Microbiology Biotechnology* 68, 533–541.
622 57. Basak, N., & Das D. (2009) Photofermentative hydrogen production using purple non-
623 sulfur bacteria *Rhodobacter sphaeroides* O.U.001 in an annular photobioreactor: A case
624 study. *Biomass Bioenergy* 33, 911–919.
625 58. Kapdan, I. K., Kargi, F., Oztekin, R., & Argun, H. (2009). Bio-hydrogen production from
626 acid hydrolyzed wheat starch by photo-fermentation using different *Rhodobacter* sp.
627 *International Journal of Hydrogen Energy* 34, 2201–2207.
628 59. Gilbert, J. J., Ray, S., & Das, D. (2011). Hydrogen production using *Rhodobacter*
629 *sphaeroides* (O.U.001) in a flat panel rocking photobioreactor. *International Journal of*
630 *Hydrogen Energy* 36, 3434-3441.

60. Kirby, A. E., Garner, K., & Levin, B. R. (2012). The Relative Contributions of Physical Structure and Cell Density to the Antibiotic Susceptibility of Bacteria in Biofilms. *Antimicrobial Agents Chemotherapy* 56, 2967–2975.

61. Montiel-Corona, V., Revah, S., & Morales, N. (2015) Hydrogen production by an enriched photoheterotrophic culture using dark fermentation effluent as substrate: Effect of flushing method, bicarbonate addition, and outdoor-indoor conditions. *International Journal of Hydrogen Energy* 40, 9096-9105.

Figure Captions:

Figure 1: Overall scheme of the developed mathematical models.

Figure 2: Attachment pattern and stages of biofilm development of *Rhodopseudomonas sp*. A) Immersion of surface modified glass plate in the culture medium; B) Irreversible Attachment; C) Proliferation; D) Maturation of the biofilm.

Figure 3: Schematic of (a) Circular and (b) Rectangular Batch Reactor for Biofilm Development.

Figure 4: Schematic of (a) Circular FPPBR and (b) Differential element of the circular FPPBR.

Figure 5: Schematic of (a) Rectangular FPPBR and (b) Differential element of the rectangular FPPBR.

Figure 6: Flow pattern of Substrate Medium inside Biofilm of *Rhodopseudomonas sp*. developed in an FPPBR.

Figure 7: Time History of Substrate (Malic Acid) in Batch Reactor.

Figure 8: Time History of Cell Density in biofilm (N)in Batch Reactor.

Figure 9: Time History of Biofilm Thicknessin Batch Reactor.

Figure 10: Biofilm Thickness-Specific Growth Rate Phase Plane Diagram when initial substrate concentration is (a) 0.5g/L; (b) 1g/L; (c) 1.5g/L and (d) 2g/L.

Figure 11: Spatial Distribution of (a) Biofilm Thickness (b) Cell Density in Biofilm (c) Substrate and (d) Hydrogen in a continuous circular FPPBR.

Figure 12: Spatial Distribution of (a) Biofilm Thickness (b) Cell Density in Biofilm (c) Substrate and (d) Hydrogen in a continuous rectangular FPPBR.

675

676

677 **Table 1: Model Constants used in the Study**

Model Parameters	Unit	Value used	Reference
μ_m	h^{-1}	0.0762	This work
K_s	g/L	1.946	This work
$Y_{X/S}$	g/g	0.55	(Uyara, Eroglu, Yucel, Gunduz, Turker, 2007)
$Y_{P/X}$	g/g	0.017	
K_{XI}	W/m^2	22	(Gadhamshetty, Sukumaran, Nirmalakhandan, Myint, 2008)
K_I	m^2/W	0.0001	
K_{PI}	W/m^2	40	
K_{pI}	m^2/W	0.001	

678

679

680

681

682

683

684

685

686

687

688

689

690

691 **Table 2: System Equations of Model for Biofilm Development in Batch Reactor**

Component	Equation used	Reference
Biomass	$\frac{dC_X}{dt} = \mu C_X = (\frac{\mu_m C_S}{K_S + C_S})C_X$	(Monod, 1942)
Substrate	$\frac{dC_S}{dt} = -\frac{1}{Y_{X/S}}\frac{dC_X}{dt}$	(Don & Shoparwe, 2010)
Product	$\frac{dC_P}{dt} = Y_{P/X}\frac{dC_X}{dt}$	(Gadhe, Sonawane, Varma, 2013)
Biofilm Thickness	$\frac{d(Th)}{dt} = p * \frac{dC_X}{dt}$	Derived in this Study
Biomass in Biofilm	$\frac{dC_{Xb}}{dt} = \mu C_{Xb}$	Derived in this Study

692

693 where, $p = \frac{V * 10^{12} * a * d}{2 * S}$

694

695

696

697

698

699

700

701

702

703

704

705

706

707

708 **Table 3: System Equations for Circular and Rectangular FPPBR**

Reactor Configuration	Component	Equation
Circular FPPBR	Biomass in Biofilm	$\frac{dC_{Xb}}{dr} = \frac{r}{u}\frac{(\mu - u)C_{Xb}}{r + R\cos(\sin^{-1}(\frac{r}{R}))}$
	Biofilm Thickness	$\frac{d(Th)}{dr} = p * \frac{dC_{Xb}}{dr}$
	Substrate	$\frac{dC_S}{dr} = -\frac{1}{Y_{X/S}}\frac{dC_{Xb}}{dr}$
	Product (H_2)	$\frac{dC_P}{dr} = Y_{P/X}\frac{dC_{Xb}}{dr} * \frac{I}{K_{PI} + I + K_{pI}I^2}$
Rectangular FPPBR	Biomass in Biofilm	$\frac{dC_{Xb}}{dx} = \frac{\mu C_{Xb}}{u * (1 - \frac{x^2\varepsilon}{S})}$
	Biofilm Thickness	$\frac{d(Th)}{dx} = p * \frac{dC_{Xb}}{dx}$
	Substrate	$\frac{dC_S}{dx} = -\frac{1}{Y_{X/S}}\frac{dC_{Xb}}{dx}$
	Product (H_2)	$\frac{dC_P}{dx} = Y_{P/X}\frac{dC_{Xb}}{dx} * \frac{I}{K_{PI} + I + K_{pI}I^2}$

709 $where, p = \frac{V * 10^{12} * a * d}{2 * S}$

710

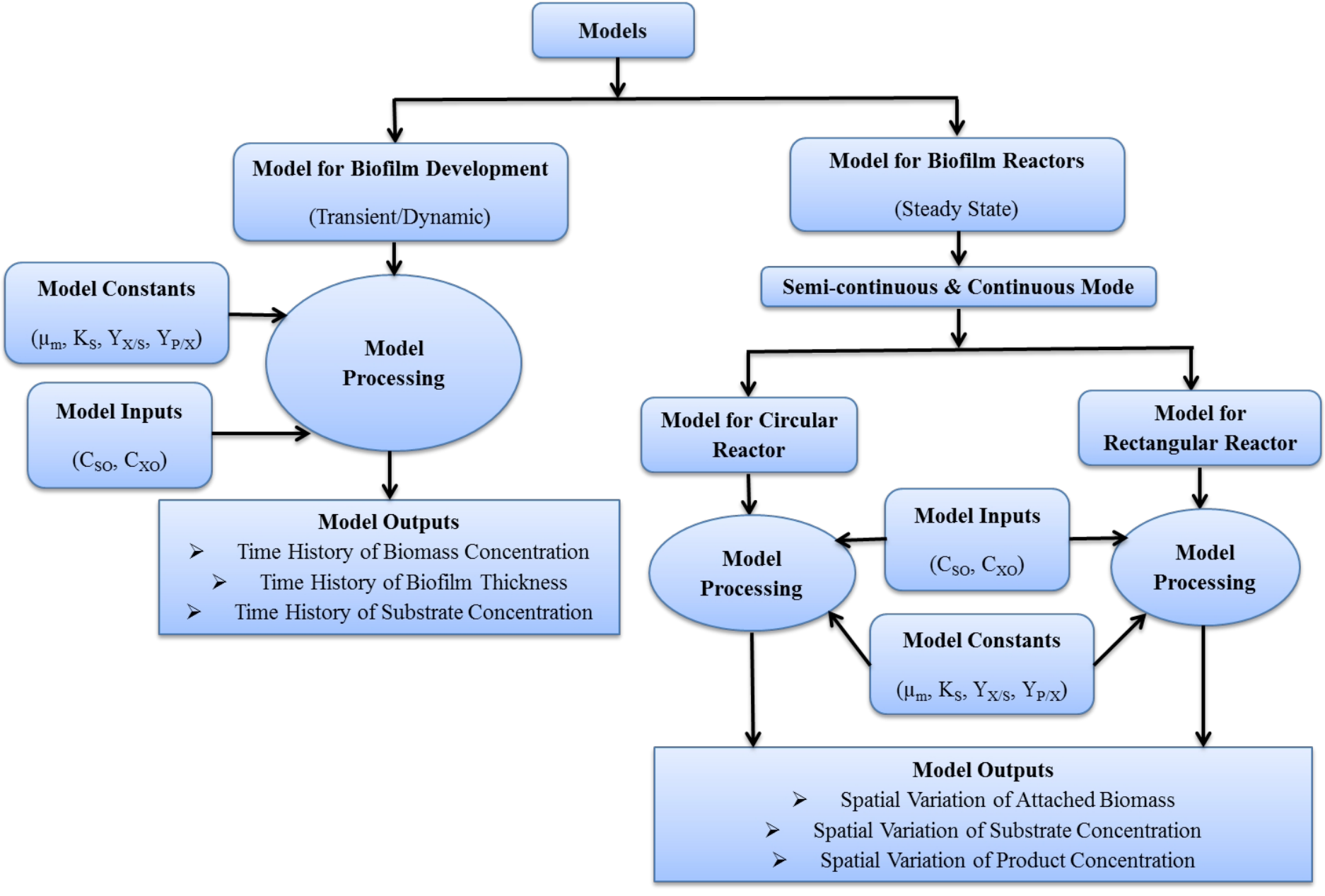
Models
Model for Biofilm Development
(Transient/Dynamic)
Model for Biofilm Reactors
(Steady State)
Model Constants
(μ_m, K_S, $Y_{X/S}$, $Y_{P/X}$)
Model Processing
Model Inputs
(C_{SO}, C_{XO})
Model Outputs
Time History of Biomass Concentration
Time History of Biofilm Thickness
Time History of Substrate Concentration
Semi-continuous & Continuous Mode
Model for Circular Reactor
Model for Rectangular Reactor
Model Processing
Model Inputs
(C_{SO}, C_{XO})
Model Processing
Model Constants
(μ_m, K_S, $Y_{X/S}$, $Y_{P/X}$)
Model Outputs
Spatial Variation of Attached Biomass
Spatial Variation of Substrate Concentration
Spatial Variation of Product Concentration

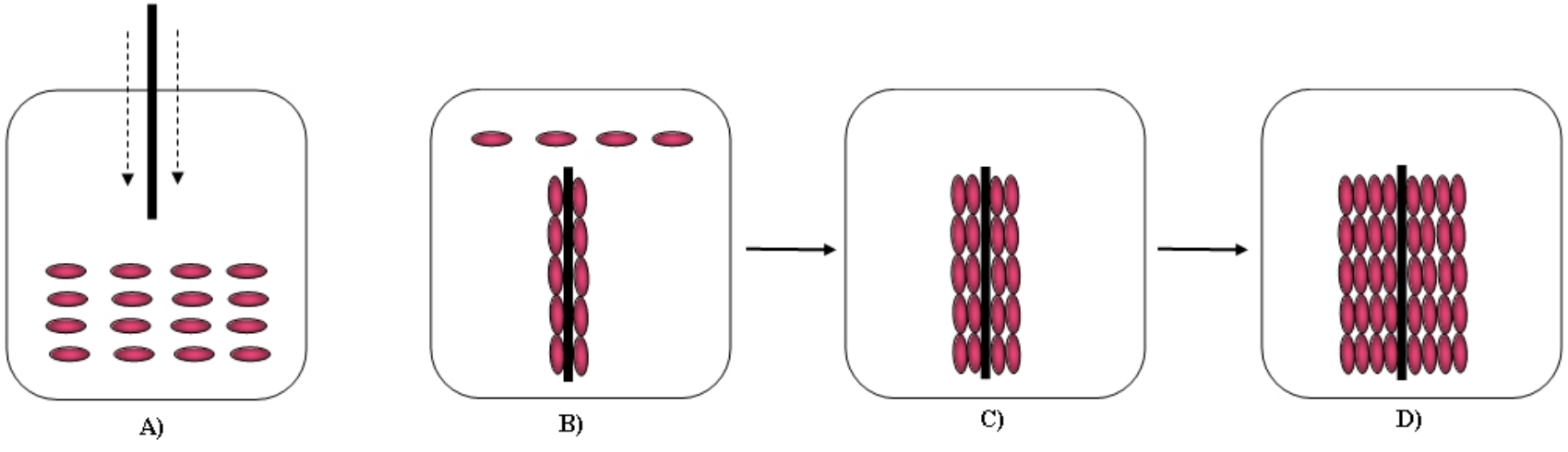

Sequential stages of biofilm development

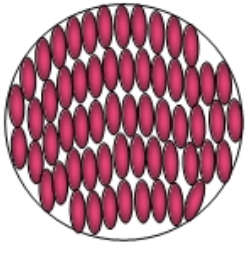

Pattern of attachment of the PNSB cells onto the glass surface

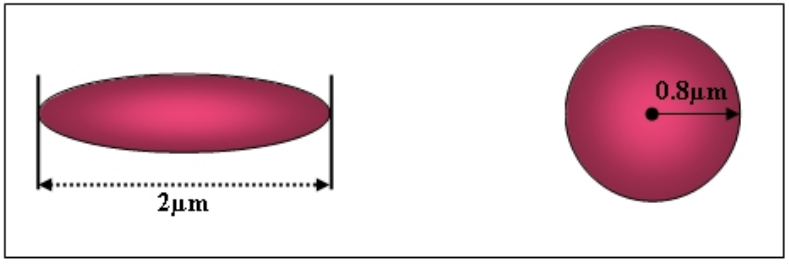

Morphological dimensions of one PNSB cell

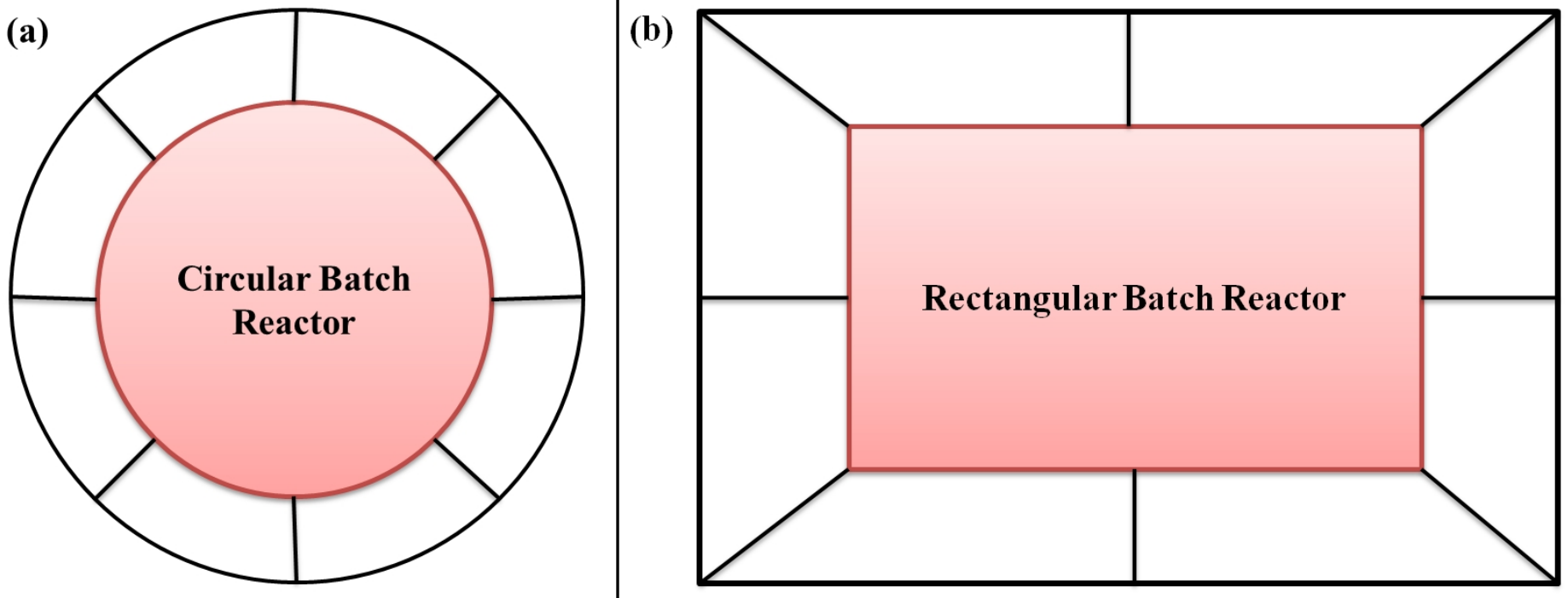
(a)
Circular Batch Reactor
(b)
Rectangular Batch Reactor

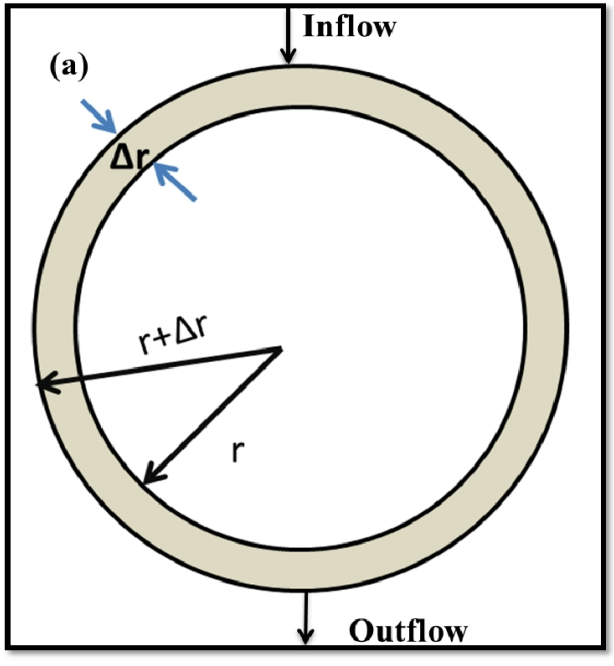
(a)
Inflow
Δr
r+Δr
r
Outflow

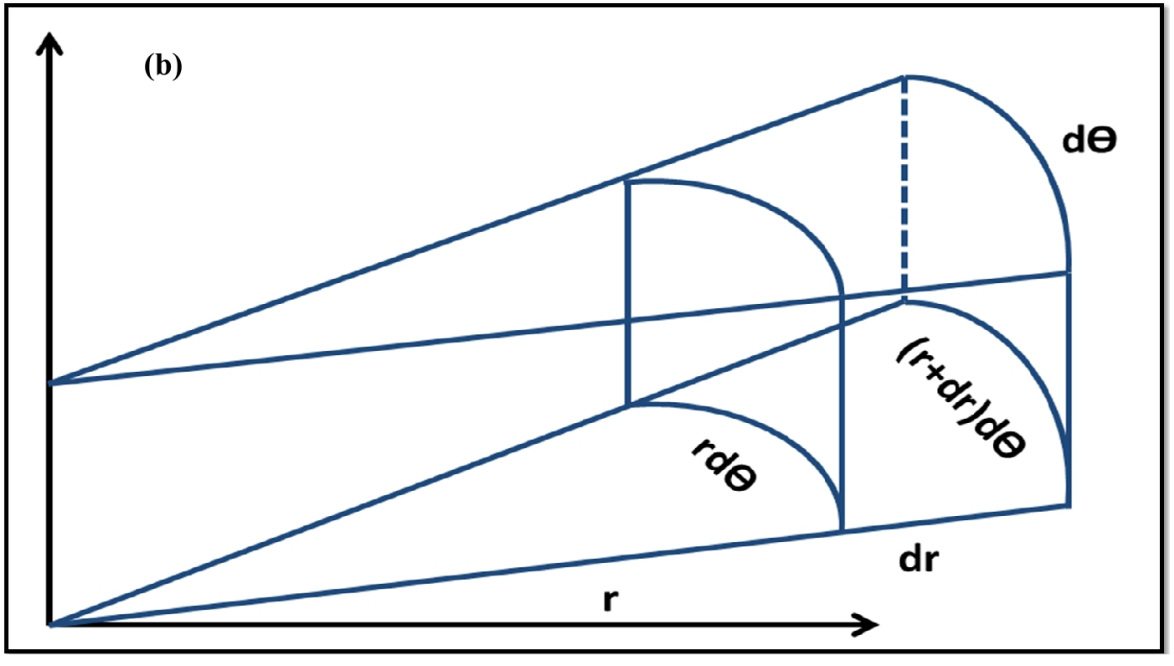
(b)
dΘ
(r+dr)dΘ
rdΘ
dr
r

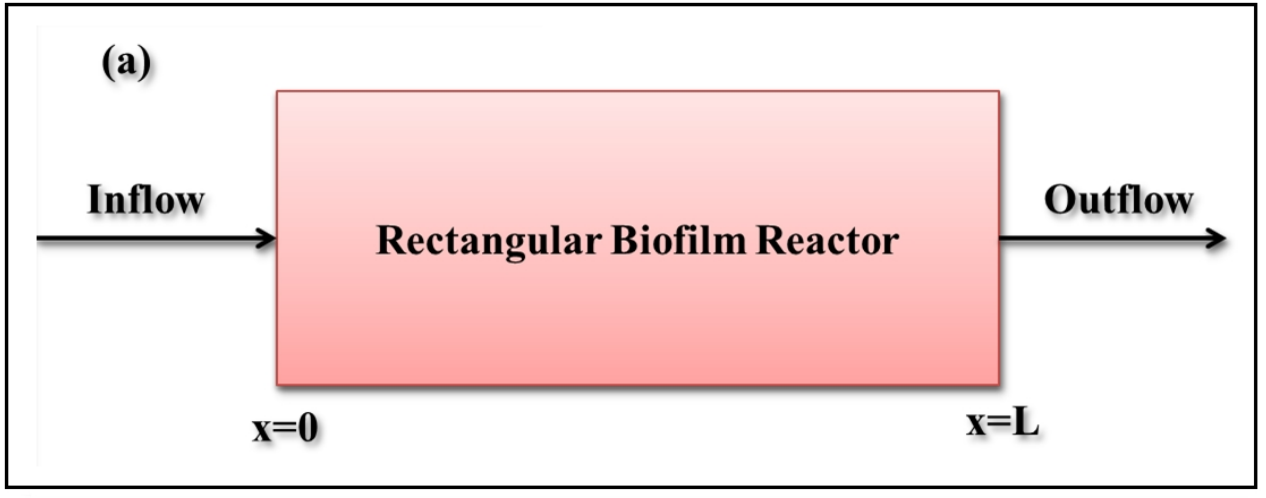
(a)
Inflow
Rectangular Biofilm Reactor
Outflow
x=0
x=L

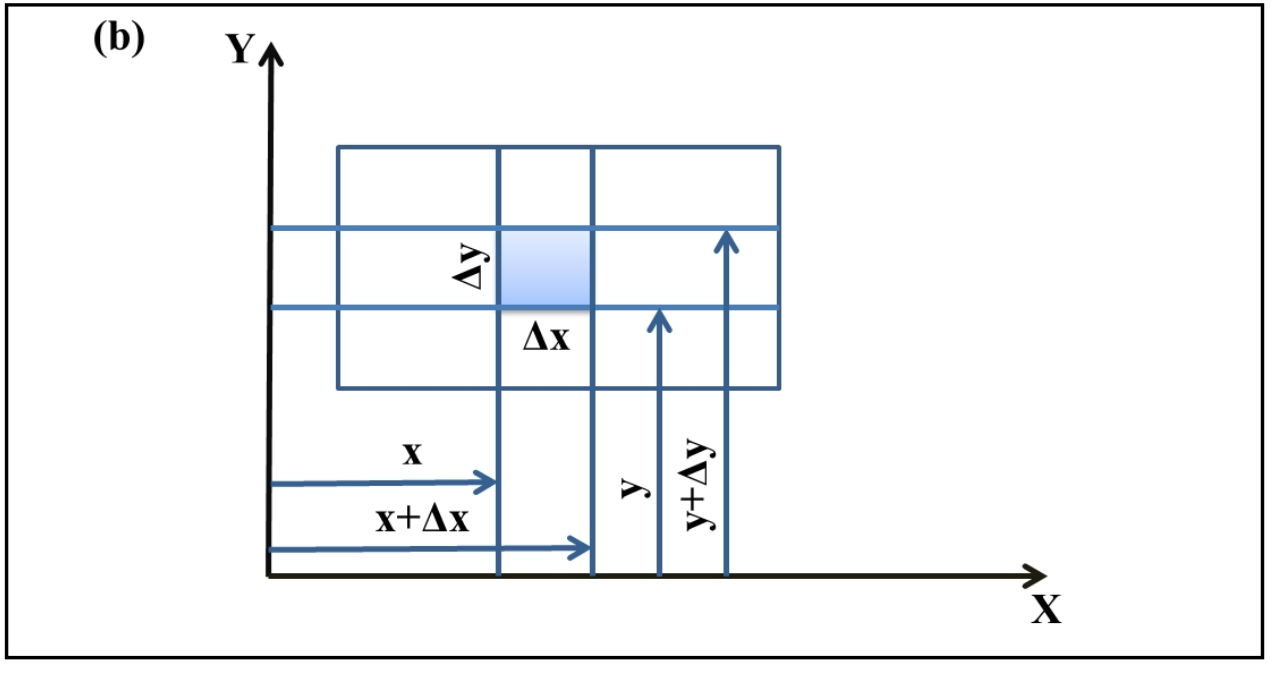
(b)
Y
Δy
Δx
x
x+Δx
y
y+Δy
X

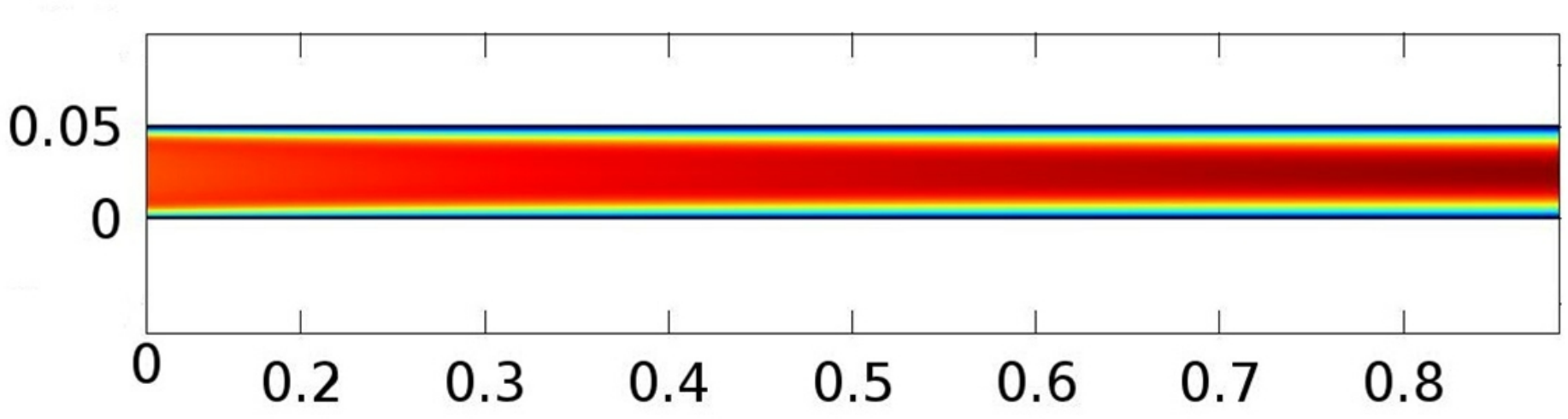
0.05
0
0
0.2
0.3
0.4
0.5
0.6
0.7
0.8

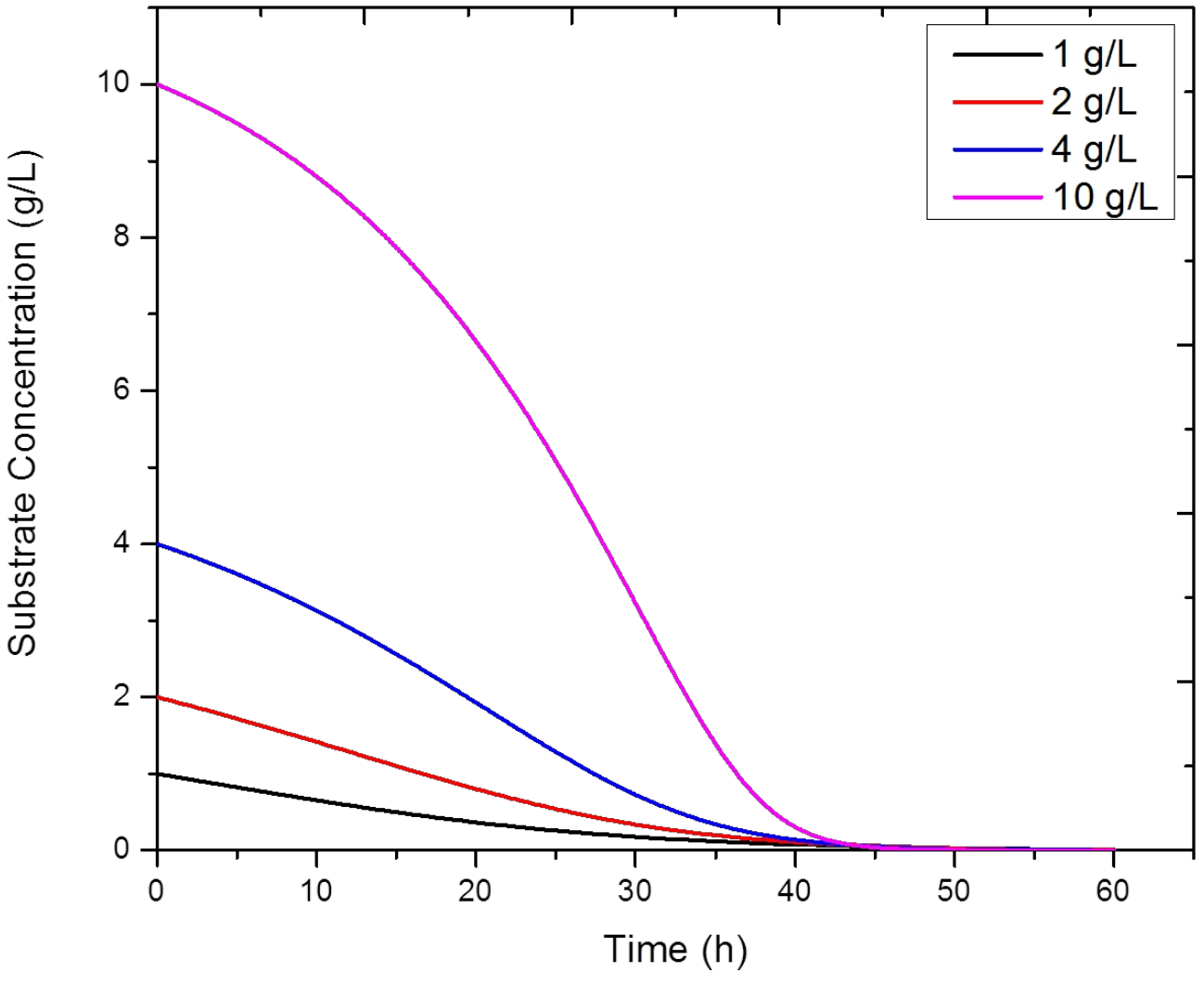
1 g/L
2 g/L
4 g/L
10 g/L
Substrate Concentration (g/L)
Time (h)
0
2
4
6
8
10
0
10
20
30
40
50
60

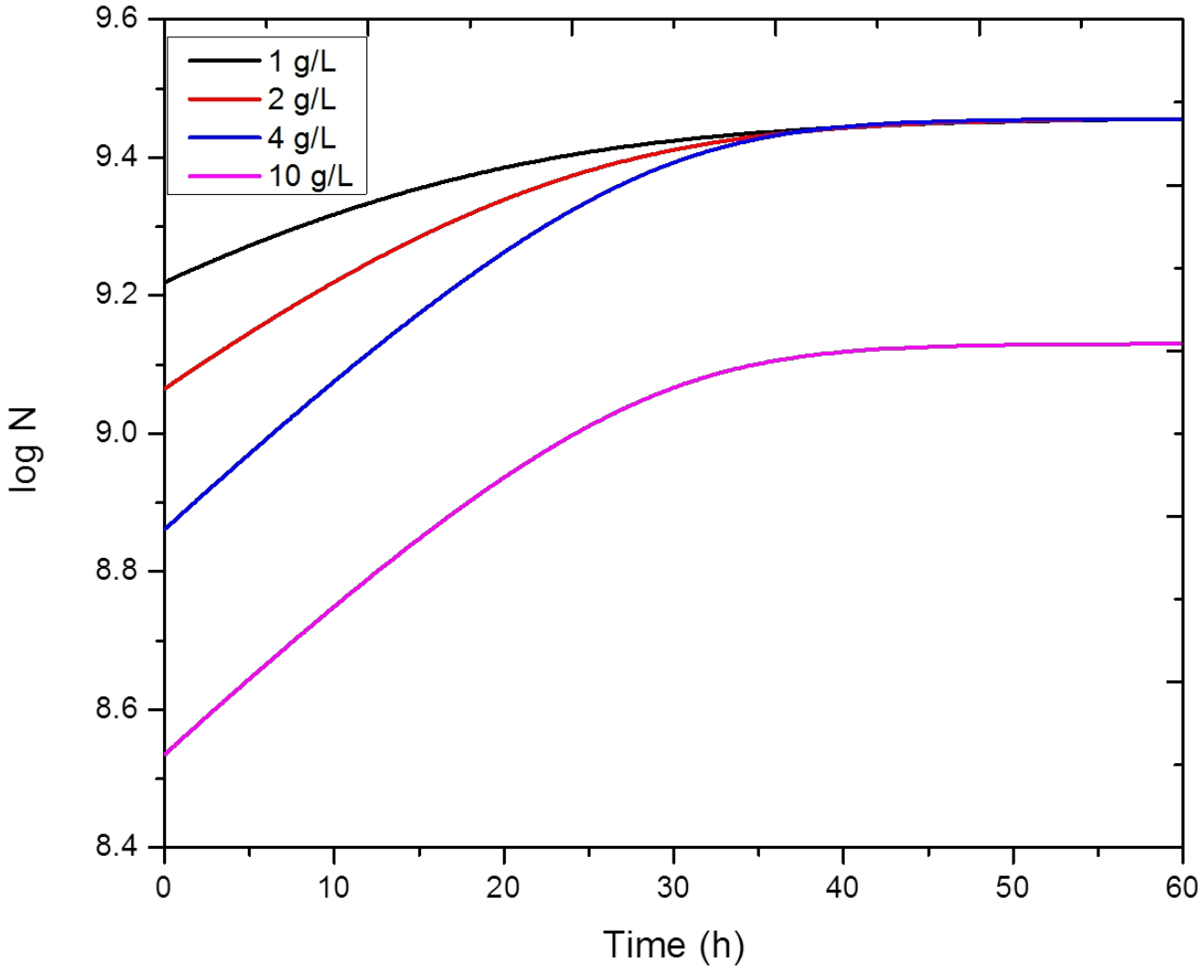
1 g/L
2 g/L
4 g/L
10 g/L
log N
Time (h)
9.6
9.4
9.2
9.0
8.8
8.6
8.4
0
10
20
30
40
50
60

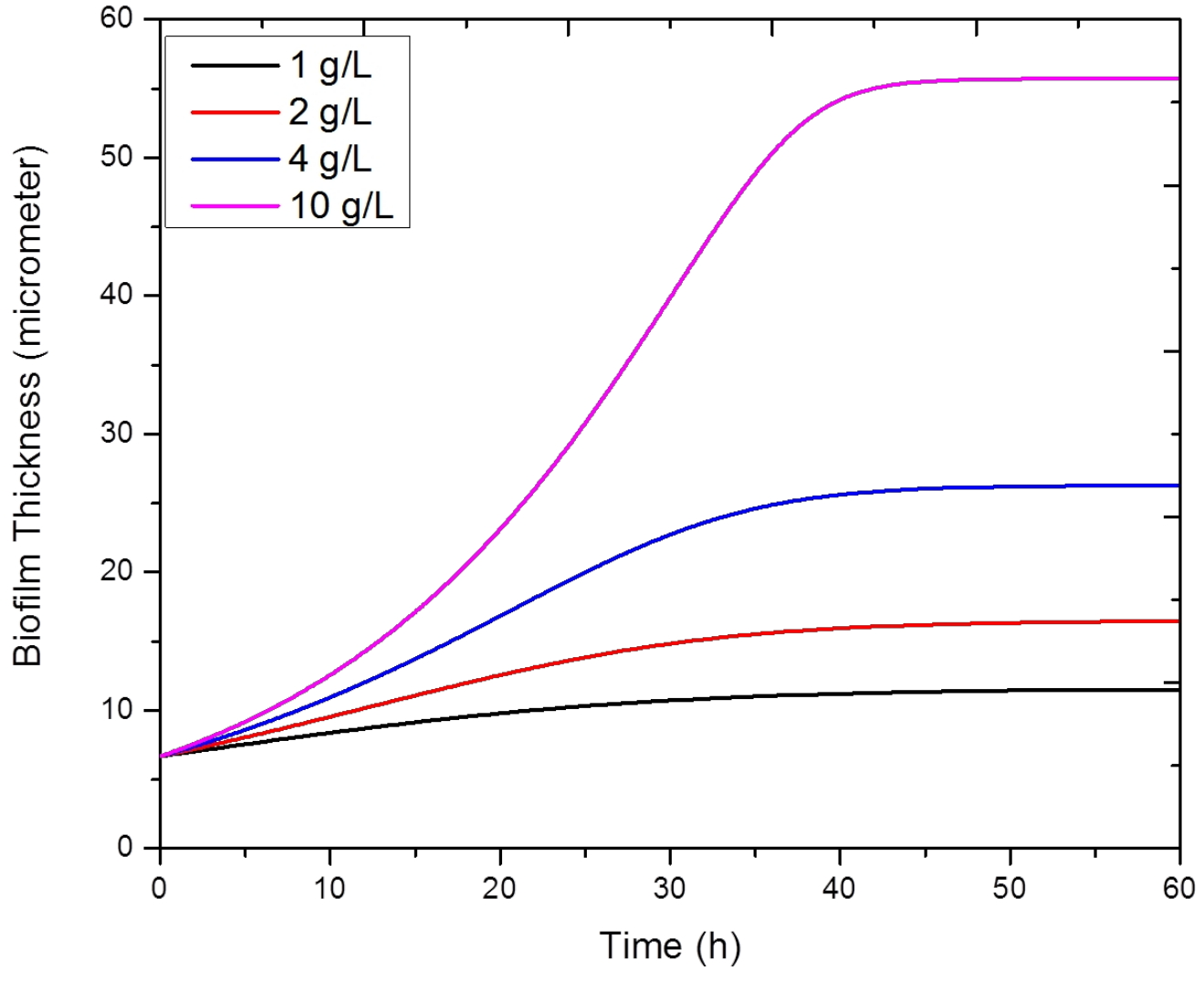
1 g/L
2 g/L
4 g/L
10 g/L
Biofilm Thickness (micrometer)
Time (h)
0
10
20
30
40
50
60

A)

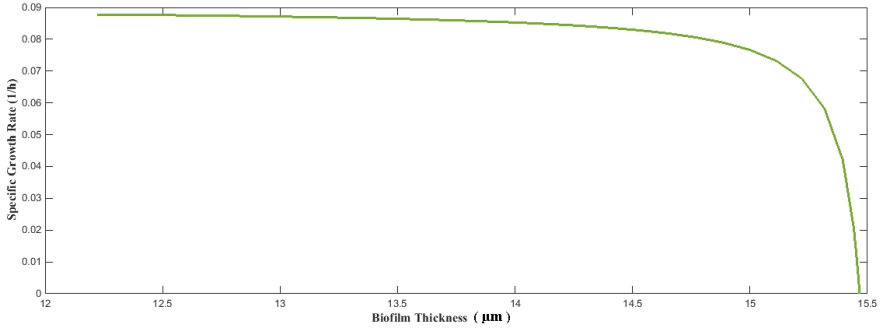
Specific Growth Rate (1/h)
Biofilm Thickness (µm)

B)

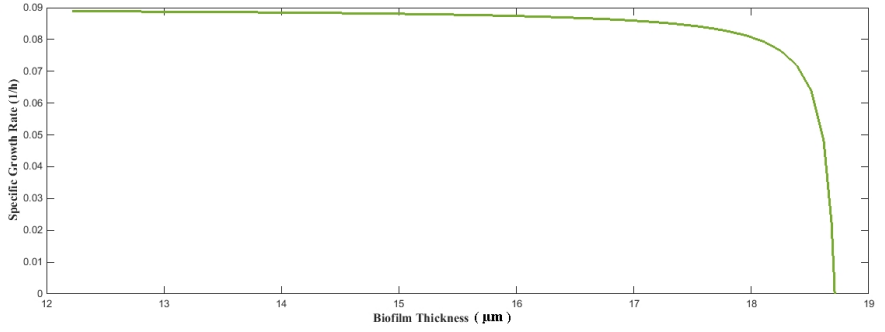
Specific Growth Rate (1/h)
Biofilm Thickness (µm)

C)

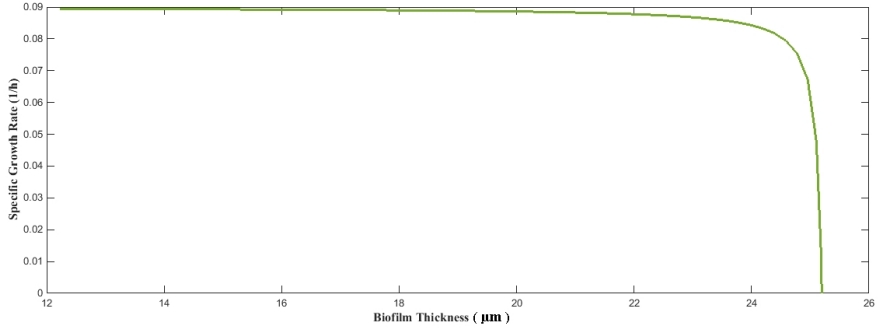
Specific Growth Rate (1/h)
Biofilm Thickness (µm)

D)

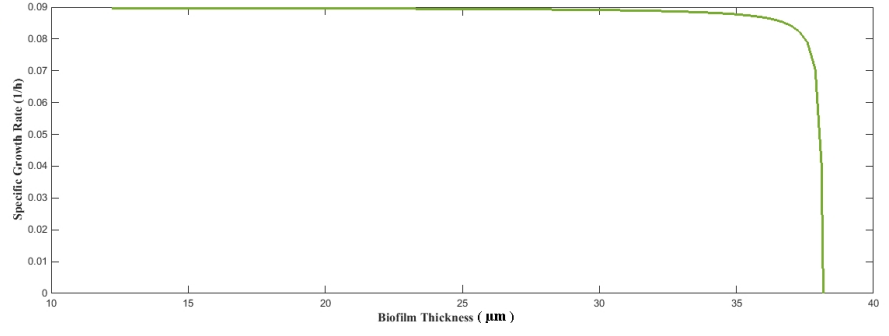
Specific Growth Rate (1/h)
Biofilm Thickness (µm)

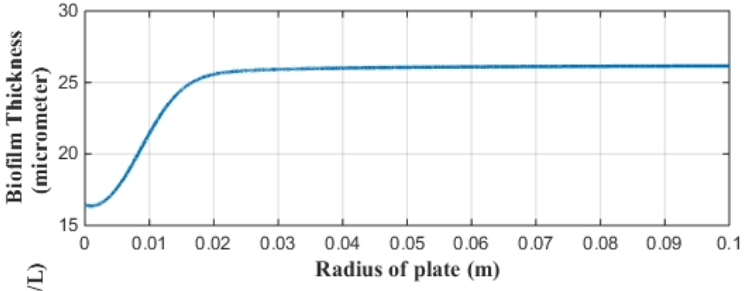
Biofilm Thickness (micrometer)
30
25
20
15
0 0.01 0.02 0.03 0.04 0.05 0.06 0.07 0.08 0.09 0.1
Radius of plate (m)

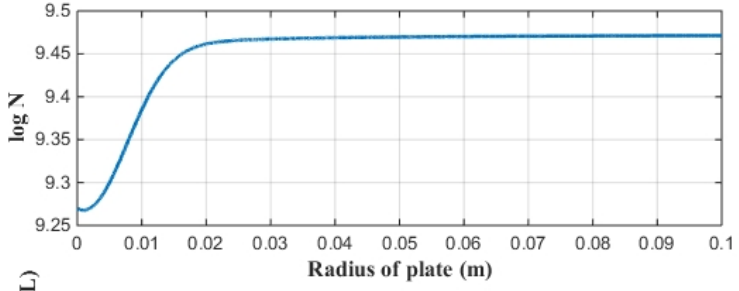
log N
9.5
9.45
9.4
9.35
9.3
9.25
0 0.01 0.02 0.03 0.04 0.05 0.06 0.07 0.08 0.09 0.1
Radius of plate (m)

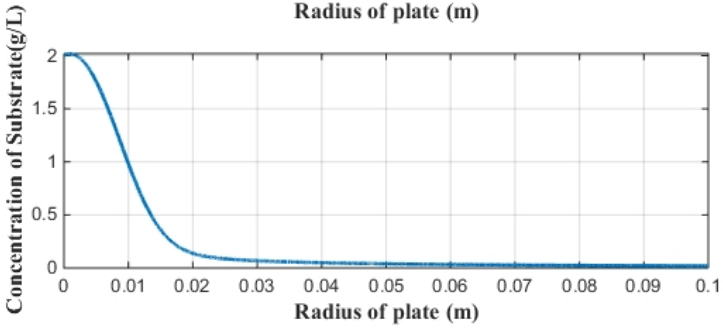
Concentration of Substrate(g/L)
2
1.5
1
0.5
0
0 0.01 0.02 0.03 0.04 0.05 0.06 0.07 0.08 0.09 0.1
Radius of plate (m)

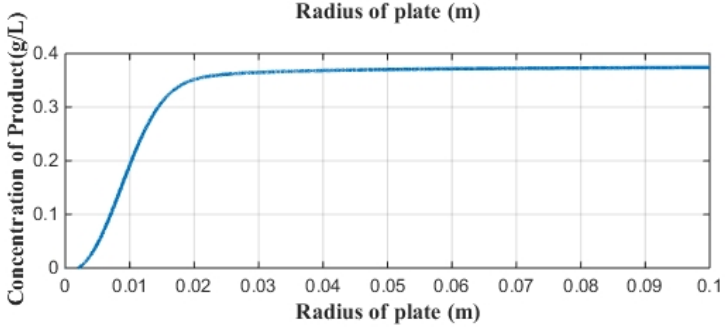
Concentration of Product(g/L)
0.4
0.3
0.2
0.1
0
0 0.01 0.02 0.03 0.04 0.05 0.06 0.07 0.08 0.09 0.1
Radius of plate (m)

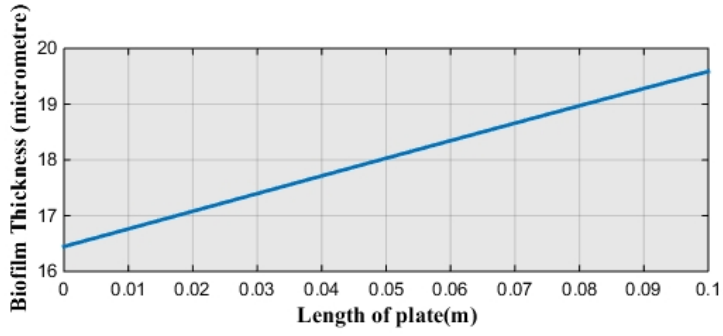
Biofilm Thickness (micrometre)
20
19
18
17
16
0 0.01 0.02 0.03 0.04 0.05 0.06 0.07 0.08 0.09 0.1
Length of plate(m)

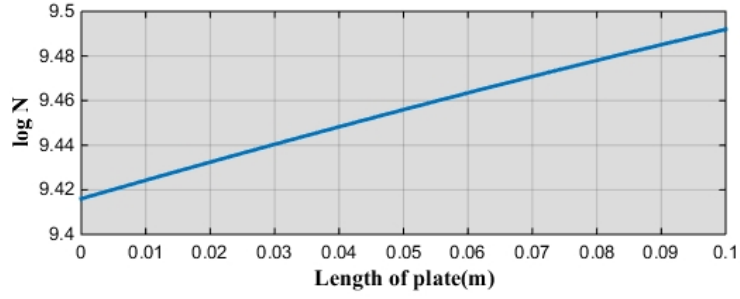
log N
9.5
9.48
9.46
9.44
9.42
9.4
0 0.01 0.02 0.03 0.04 0.05 0.06 0.07 0.08 0.09 0.1
Length of plate(m)

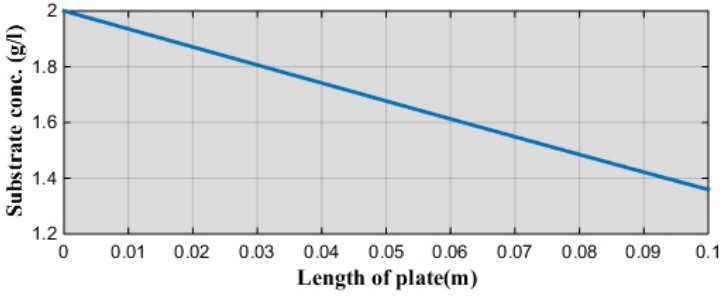
Substrate conc. (g/l)
2
1.8
1.6
1.4
1.2
0 0.01 0.02 0.03 0.04 0.05 0.06 0.07 0.08 0.09 0.1
Length of plate(m)

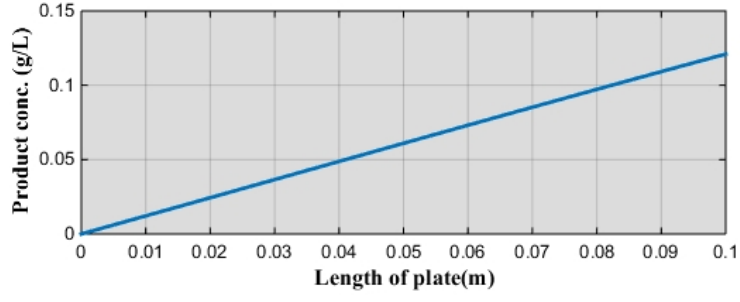
Product conc. (g/L)
0.15
0.1
0.05
0
0 0.01 0.02 0.03 0.04 0.05 0.06 0.07 0.08 0.09 0.1
Length of plate(m)